Experimental Constraints on the Relationships between Peralkaline Rhyolites of the Kenya Rift Valley

Bruno Scaillet, Ray Macdonald

JOURNAL OF PETROLOGY | VOLUME 44 | NUMBER 10 | PAGES 1867–1894 | 2003 | DOI: 10.1093/petrology/egg062

Experimental Constraints on the Relationships between Peralkaline Rhyolites of the Kenya Rift Valley

BRUNO SCAILLET[1]* AND RAY MACDONALD[2]

[1]INSTITUT DES SCIENCES DE LA TERRE D'ORLÉANS, CNRS, 1A RUE DE LA FÉROLLERIE, 45071, ORLÉANS CEDEX 02, FRANCE

[2]ENVIRONMENT CENTRE, LANCASTER UNIVERSITY, LANCASTER LA1 4YQ, UK

RECEIVED MAY 13, 2002; ACCEPTED APRIL 15, 2003

Crystallization experiments on three comendites provide evidence for the genetic relationships between peralkaline rhyolites in the central Kenya rift valley. The crystallization of calcic clinopyroxene in slightly peralkaline rhyolites inhibits increase in peralkalinity by counteracting the effects of feldspar. Fractionation under high fO_2 conditions produces residual liquids that are less, or only slightly more, peralkaline than the bulk composition. In contrast, crystallization under reduced conditions (<FMQ, where FMQ is the fayalite–magnetite–quartz buffer) and at high fF_2 inhibits calcic clinopyroxene and yields residual liquids that are more peralkaline than coexisting alkali feldspar, whose subsequent crystallization increases the peralkalinity of the liquid. A marginally peralkaline rhyolite [molar $(Na_2O + K_2O)/Al_2O_3$ (NK/A) = 1·05] can yield a more typically comenditic rhyolite (NK/A = 1·28) after 95 wt % of crystallization. This comendite yields pantelleritic derivatives (NK/A > 1·4) after 25 wt % crystallization. Upon further crystallization, extreme peralkaline compositions (NK/A ≤2·5) are obtained, with relatively low SiO_2 (66 wt %) and Al_2O_3 (7·4 wt %), and high FeO (10·2 wt %) and Na_2O (8·4 wt %) contents. In the absence of crystallization of sodic phases such as arfvedsonite or aegirine, fractionation may yield even more extreme compositions. Pantelleritic rhyolites can be produced at temperatures below 800°C, at low fO_2, high fF_2, by either extreme fractional crystallization or near-solidus melting of less peralkaline, but more silicic, sources.

KEY WORDS: *peralkaline rhyolites; redox state; magmatic differentiation; Kenya rift*

INTRODUCTION

Peralkaline rocks have, by definition, a molar excess of $(Na_2O + K_2O)$ over Al_2O_3. Overwhelmingly they are of salic composition, i.e. trachytes, rhyolites and phonolites. Such rocks commonly occur, in both continental and oceanic settings, as the relatively low-volume end-products of protracted fractional crystallization of alkali basalt magmas (Barberi *et al.*, 1975; Smith *et al.*, 1977; McDonough & Nelson, 1984; Novak & Mahood, 1986; Mungall & Martin, 1995; Civetta *et al.*, 1998; Kar *et al.*, 1998). They also occur in bimodal associations with flood basalts, such as the Ethiopian traps (Ayalew *et al.*, 2002). However, in some volcanoes and volcanic fields, peralkaline salic rocks can be the dominant eruptive product (Macdonald, 1987; Macdonald *et al.*, 1987; Henry *et al.*, 1990; Horn & Schmincke, 2000).

In such cases, the large volumes relative to mafic and intermediate rocks cannot easily be ascribed to fractional crystallization of basaltic magma and, accordingly, models have been developed whereby peralkaline salic rocks have been formed by partial melting of crustal rocks, ranging from under-plated basalts (Bailey & Schairer, 1966; Macdonald *et al.*, 1970; Lowenstern & Mahood, 1991; Bohrson & Reid, 1997, 1998) to high-level, more silicic rocks (Bailey & Macdonald, 1969; Davies & Macdonald, 1987; Macdonald *et al.*, 1987; Mahood & Halliday, 1988; Scaillet & Macdonald, 2001). So far as we are aware, however, no experimental study of crustal anatexis has yet produced peralkaline melts. Thus several studies

*Corresponding author. E-mail: bscaille@cnrs.orleans.fr

have invoked volatile-fluxed melting, involving especially halogens, which occur in relatively high concentrations in peralkaline magmas, as a way of adding alkalis to the protoliths (Macdonald *et al.*, 1970, 1987; Bailey & Macdonald, 1975, 1987). There is, as yet, no confirmatory experimental evidence that this mechanism is viable.

Peralkaline, silica-oversaturated, extrusive rocks are classified into four types: comenditic trachytes, pantelleritic trachytes, comendites and pantellerites (Macdonald, 1974). The pantelleritic types are invariably richer in Na and Fe, and poorer in Al, than their comenditic equivalents. Genetic relationships between the magma types are variable. Civetta *et al.* (1998) suggested that pantellerites from the type locality of Pantelleria were formed by the closed-system fractional crystallization of comenditic trachytes, whereas Lowenstern & Mahood (1991) recognized the lineage pantelleritic trachyte–pantellerite from the same island. Bohrson & Reid (1997) reported the fractionation sequence comenditic trachyte–pantelleritic trachyte–pantellerite from Socorro Island, Mexico. On Ascension Island, comenditic trachytes are thought to have been parental to comendites (Kar *et al.*, 1998).

In this paper we document, for the first time, the formation of strongly peralkaline, pantelleritic melts by crystallization of high-silica comendites. The comendites are natural obsidians from the south–central Kenya rift, which, on the basis of isotopic and trace element data, are thought to have formed by partial melting of crustal rocks (Bailey & Macdonald, 1969; Davies & Macdonald, 1987; Macdonald *et al.*, 1987; Black *et al.*, 1997; Heumann & Davies, 2002). We infer that, in this case at least, pantelleritic melts showing extreme Fe enrichment and Al depletion are the result of protracted crystallization of high-silica anatectic magmas.

GEOLOGICAL OUTLINE

The volcanic complexes of interest here, Olkaria and Eburru, lie in the south–central part of the Kenya rift and are the only centres in the Kenya rift where rhyolitic volcanism is still active (Fig. 1). They are located, along with the peralkaline trachyte caldera volcano Longonot, within an area of 50 km × 30 km, a much greater concentration of Pleistocene to Recent volcanoes than elsewhere in the Rift (Clarke *et al.*, 1990). To the south lies the peralkaline trachyte–phonolite caldera volcano Suswa (Fig. 1).

The Greater Olkaria Volcanic Complex is a young (<20 ka), multicentred volcanic field, 240 km^2 in area, lying to the west and south of Lake Naivasha, east of Nairobi. The complex is dominated by steep-sided domes composed of lava and/or pyroclastic rocks and

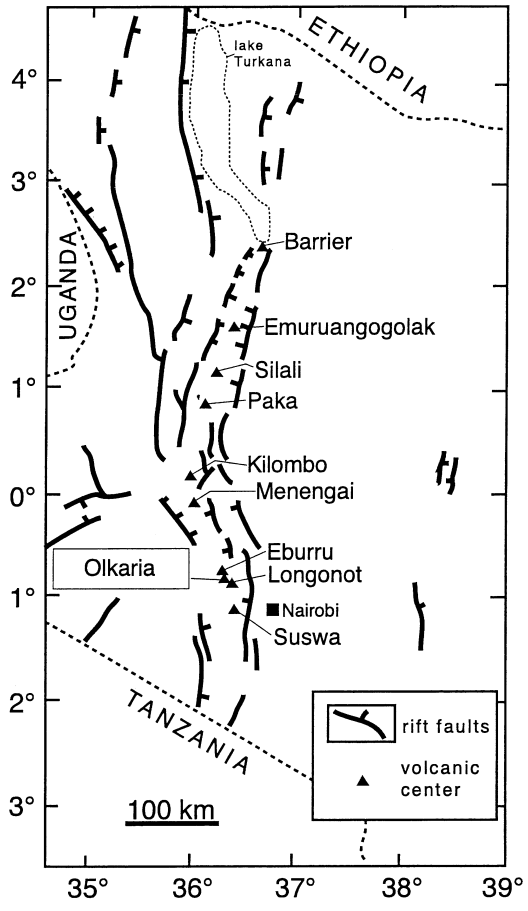

Fig. 1. Locality map of the Olkaria and Eburru rhyolitic complexes and of the nearby trachytic caldera volcanoes Longonot and Suswa. Also shown are the main volcanic centres of the Kenya rift zone.

by thick lava flows of restricted lateral extent (Clarke *et al.*, 1990). The great majority of the rocks are mildly peralkaline rhyolites, plotting in the comendite field of the FeO*–Al_2O_3 classification diagram of Macdonald (1974) (Fig. 2). However, some early extrusives erupted in the northern and southern parts of the complex are more strongly peralkaline and may be termed pantellerites (Fig. 2).

The Eburru Volcanic Complex is located to the NW of Lake Naivasha. Its southern boundary coincides with the northern boundary of the Olkaria field. Its age is not known in detail but all units are <0·45 Ma, and the youngest eruptives probably no more than a few hundred years old (Clarke *et al.*, 1990). Lithologically, Eburru is composed almost entirely of peralkaline trachytes and rhyolites of pantelleritic affinity (Fig. 2). Two groups, members of which have been erupted throughout the history of the complex, have been distinguished by Clarke *et al.* (1990); the Eburru Trachyte and the Eburru Pantellerite. On the FeO*–Al_2O_3 plot, the Eburru Trachyte straddles

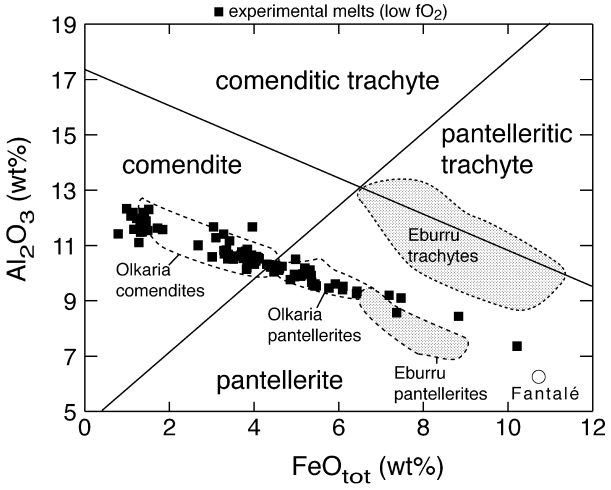

Fig. 2. Fields of Olkaria and Eburru volcanic rocks (Clarke *et al.*, 1990) in the FeO^*–Al_2O_3 classification diagram of Macdonald (1974). Also shown are the experimental melts (glasses, ■) obtained in this study from crystallization of ND002, BL575 and SMN49 under low fO_2 conditions. A natural pantelleritic obsidian from the Fantalé volcano, Ethiopia (Lacroix, 1930) is also shown.

the boundary between pantelleritic trachyte and pantellerite, whereas the Eburru Pantellerite plots entirely within the pantellerite field, parallel to, but displaced below, the Eburru Trachyte (Fig. 2).

On the basis of these geochemical relationships, it would appear that magmas of Eburru Trachyte type are unlikely to have been parental to the Eburru Pantellerite, a conclusion already drawn by Macdonald *et al.* (1970) from alkali feldspar–melt relationships. However, the linear relationship between the Olkaria comendites, Olkaria pantellerites and the Eburru pantellerites raises the possibility that the pantellerites have formed by crystallization or melting of comendites similar in major element composition to the Olkaria rhyolites. In this paper, we test that possibility experimentally.

EXPERIMENTAL AND ANALYTICAL TECHNIQUES

Complete details of the experimental and analytical techniques used in this study have previously been given by Scaillet & Macdonald (2001) and only a general overview is provided here. Experiments were conducted on three phenocryst-poor comenditic obsidians (ND002, BL575, SMN49) from the Greater Olkaria Volcanic Complex. The rocks have agpaitic indices [molar $(Na_2O + K_2O)/Al_2O_3$, subsequently abbreviated to NK/A] between 1·05 and 1·36 and thus cover most of the compositional range in the Olkaria comendites. Geochemical and modal data for the samples have been given by Macdonald *et al.* (1987) and Scaillet & Macdonald (2001). In summary, ND002 (NK/A 1·05) contains <5% (volume) phenocrysts of alkali feldspar, clinopyroxene, fayalite, magnetite, zircon, apatite and a mineral of the chevkinite group. BL575 is the most peralkaline of the three samples (NK/A 1·36) and contains 5% phenocrysts of alkali feldspar, riebeckite–arfvedsonite, aenigmatite, biotite, ilmenite and a chevkinite-group mineral. SMN49 is compositionally very similar to BL575, being only slightly more SiO_2 rich and less peralkaline (NK/A 1·31), but has a different phenocryst assemblage, containing fluorite and lacking riebeckite and aenigmatite.

All experiments were conducted in cold seal pressure vessels. Pressure and temperature uncertainties are ±3 MPa, and ±8°C, respectively. Redox conditions were evaluated either with H_2-membranes (low oxygen fugacity, fO_2) or with NiPd solid sensors (high fO_2), and by determining the Fe^{2+}/Fe^{3+} ratio of test experiments. Run durations varied between 7 and 40 days, depending on temperature. Experiments were performed at 150 and 50 MPa, in the temperature range 660–800°C. Melt H_2O contents varied from 1 to 6 wt %. At 150 MPa, both low (NNO − 1·63, i.e. 1·63 log units below the Ni–NiO buffer) and high (NNO + 3·63) fO_2 conditions were investigated. The phase relationships of all three samples were reported by Scaillet & Macdonald (2001).

Run products were characterized by scanning electron microscopy (SEM) and electron microprobe analysis (EMPA). Analytical conditions for EMPA were accelerating voltage 15 kV, sample current 6 nA, counting time 10 s on peak for all elements and a focused beam for minerals. For glasses, the beam was defocused to 5 μm. Na and K were analysed first and a ZAF correction procedure was applied. Melt H_2O contents were determined using the by-difference method (Devine *et al.*, 1995) and are considered accurate to 0·6 wt % absolute.

Problems of Na migration under the electron beam were found to be most acute in strongly peralkaline, hydrous compositions. Correction factors for Na loss were based on analysis of synthetic peralkaline rhyolitic compositions and a set of metaluminous rhyolitic glasses, all of known composition. At the beginning of each analytical session, both sets of standards were analysed, the metaluminous standards being used for retrieving the Na correction factor for ND002 and the peralkaline standards for BL575 and SMN49.

Contamination of some runs by Ni from the vessel was reported by Scaillet & Macdonald (2001), who suggested that the contamination was not instrumental in crystal growth. Here we discuss only mineral compositions free of Ni contamination, with the exception

of some analyses representing scarce amphibole in ND002.

Systematic SEM processing of the charges shows that the feldspar is on average homogeneous. There are two exceptions, however. The first concerns the largest crystals that sometimes display zoning. Electron microprobe traverses show that this zoning is most often from potassic cores toward sodic rims, but the reverse is occasionally observed. The core to rim compositional range is normally on the order of 5–6 mol % Ab, but in a few cases reaches 10 mol % Ab. Similarly, large feldspars crystallized under high fO_2 in BL575 and SMN49 display a marked iron enrichment toward the rim, typically from 1 to 2–3 wt % Fe_2O_3. In all cases, however, the rim composition of the large crystals is identical to that of the smallest individuals, the latter accounting for >90% of the feldspar population. This type of zoning in experimentally produced feldspars has also been observed in crystallization experiments on a metaluminous dacite, using the same experimental procedure as in this study (Scaillet & Evans, 1999). The occurrence of large zoned feldspar crystals in crystallization experiments using dry glass as starting material has been interpreted as the result of feldspar nucleation and growth before attainment of equilibrium conditions, in particular for fH_2O and fO_2. This interpretation also appears to hold here. Growth of feldspar during transient conditions where the melt water content is significantly lower than at equilibrium, and thus when lower fO_2 prevails, readily explains the observed iron zonation, the iron-poor core characterizing more reducing conditions during crystal growth than the iron-rich rim. Indeed, the experimental results clearly show that the iron content of feldspar increases with fO_2. Similarly, the potassic core would also mark water-poor conditions relative to the sodic rim.

The second type of feldspar heterogeneity occurs at 150 MPa, at T <700°C, where several charges displayed substantial variation in feldspar composition, notably in compositions BL575 and SMN49. Typically, several analyses performed in a single charge display a continuous trend in Na/K ratio (usually over 10 mol % Ab), independent of the size of the analysed crystal and therefore unlike the zoning associated with the large crystals described above. It was not possible to retrieve from these low-temperature charges a meaningful average feldspar composition. We suggest that part of this compositional variation may be due to experimental conditions lying below the crest of the alkali feldspar solvus. At 150 MPa, the crest of the disordered alkali feldspar solvus is around 670°C (Luth *et al.*, 1974). However, this is a likely minimum value, as it is known that the solvus widens and rises with ordering of alkali feldspars. Our experimental conditions, including long run durations (e.g. Martin, 1974), high fH_2 (Goldsmith & Jenkins, 1985) and the peralkaline nature of the starting material (Martin, 1974), promote ordering of alkali feldspars (Goldsmith & Newton, 1974; Parsons, 1978). In addition, the position of the solvus has been determined in iron-free systems, whereas the experimental feldspars contain around 1 wt % Fe_2O_3 under reducing conditions. It may well be that iron raises the crest of the solvus.

For these reasons, we tentatively suggest that some of the low-temperature charges may have been slightly below the solvus, with the consequence of crystallizing two alkali feldspars instead of one. In such an event, because the conditions probably lie in the upper reaches of the solvus, the compositions of the coexisting feldspars do not appreciably differ from each other, which explains the difficulty in contrasting them on SEM images. Unfortunately, by the time this problem was appreciated, there was insufficient run product left over after probe mount preparation and we could not perform X-ray measurements to test this hypothesis. Therefore, instead of an average, for such charges we provide the two end-member feldspar compositions (see Table 2, below). At 50 MPa, no such problem was encountered, consistent with the fact that the solvus crest goes down temperature as pressure decreases (16°C/100 MPa, Goldsmith & Newton, 1974; Parsons, 1978). The compositions of both types of heterogeneous feldspar are, however, omitted from the discussion.

RESULTS

Proportions of phases

Phase proportions have been calculated using a constrained least-squares mass balance with propagation of analytical errors of the experimental phases (Albarède, 1995), using all major elements except volatiles (Table 1). Apart from four of the charges, residuals are always significantly below unity. This suggests that no major phase has been overlooked and that the Na contents of the quenched melts have been correctly evaluated. The low residuals also confirm that iron loss to the capsule container was negligible under the chosen experimental conditions (<6% of the original FeO*).

Quartz and feldspar usually comprise >95 wt % of the phase assemblage. Their abundances increase linearly as the melt fraction decreases (Fig. 3). Upon complete crystallization, all three compositions have similar modal compositions, with 67–70 wt % feldspar and 30–32 wt % quartz. Except at near-liquidus conditions in ND002, the feldspar/quartz mass ratio is two

Table 1: Proportions of phases (wt %) in selected run products

	P (MPa)	*T* (°C)	ΔNNO[1]	gl	af	qtz	cpx	amph	fay	ox	bt/mdt	fl	chek/tit	r^2
ND002														
3	156	788	−1·37	85·24	9·85	2·97	1·72	—	—	0·22	—	—	—	0·01
7	161	738	−1·14	92·37	5·85	0·10	1·54	—	—	—	—	—	—	0·07
8	148	699	−1·12	98·14	—	—	1·49	—	—	0·37	—	—	—	0·27
9	148	699	−1·22	80·97	13·33	2·93	2·47	—	—	0·31	—	—	—	0·05
10	50	794	−1·48	99·55	—	—	0·27	—	—	0·18	—	—	—	0·64
11	50	794	−1·67	90·36	8·02	—	1·27	—	—	0·35	—	—	—	0·26
15	155	794	4·06	94·86	4·23	—	0·45	—	—	0·45	—	—	—	0·05
16	155	794	3·93	83·90	13·70	1·23	0·38	—	—	0·75	—	0·04	—	0·07
17	152	752	4·29	99·47	—	—	—	—	—	0·38	—	—	0·16	0·58
18	152	752	4·19	92·85	5·85	—	0·37	—	—	0·56	—	—	0·36	0·02
19	152	752	4·10	88·50	10·10	—	0·70	—	—	0·66	—	—	0·17	0·04
20	152	752	3·96	31·37	46·42	20·11	0·70	—	—	1·02	—	—	0·38	0·02
21	152	752	3·86	0·93	69·09	27·60	1·19	—	—	1·19	—	0·01	—	0·02
22*	149	788	−1·80	61·90	26·70	9·00	2·20	—	—	0·20	—	—	—	0·02
23*	155	696	4·17	95·88	2·39	—	0·57	—	—	0·87	—	—	0·29	0·48
24	155	696	4·08	69·86	21·22	6·85	1·11	—	—	0·96	—	—	—	0·26
25	155	696	3·97	31·32	45·48	20·52	1·84	—	—	0·85	—	—	—	0·24
28*	52	790	−1·82	82·53	15·53	—	1·44	—	—	0·51	—	—	—	0·83
29*	52	790	−1·94	71·40	23·86	2·92	1·42	—	—	0·41	—	—	—	0·43
30*	52	790	−2·11	70·90	19·80	7·60	1·40	—	—	0·30	—	—	—	0·50
33	156	693	−1·82	0·10	66·20	30·97	—	—	2·06	0·34	0·01	0·44	—	0·18
34*	57	756	−1·36	88·36	9·72	—	1·55	—	—	0·37	—	—	—	0·54
35	57	756	−1·54	38·60	42·18	17·49	1·41	—	—	0·33	—	—	—	0·31
38	150	784	2·35	48·83	36·37	14·08	—	—	—	0·40	—	0·33	—	0·26
42	152	758	−3·13	12·65	58·66	26·75	—	0·01	1·64	0·31	—	0·01	—	0·35
43	152	729	−3·20	12·49	59·42	26·42	—	—	1·36	0·31	0·01	0·01	—	0·49
44*	152	773	−3·10	41·63	38·69	18·74	—	0·01	0·74	0·21	0·01	0·01	—	0·25
BL575														
16	155	805	3·12	98·59	—	1·15	—	—	—	0·26	—	—	—	0·10
21	152	757	3·04	96·13	2·35	1·02	—	—	—	0·36	—	0·14	—	0·31
22	149	788	−1·86	99·99	—	0·05	—	—	—	0·05	—	—	—	—
23	149	791	−2·06	50·43	32·12	17·45	—	—	—	—	—	—	—	0·06
24	149	791	−2·30	34·47	43·32	22·21	—	—	—	—	—	—	—	0·15
25	155	703	3·39	99·21	—	—	—	—	—	0·79	—	—	—	0·00
26	155	703	3·27	99·20	—	—	—	—	—	0·80	—	—	—	0·00
27	155	703	3·17	91·10	4·51	3·56	—	—	—	0·84	—	—	—	0·02
28	155	703	3·04	77·94	13·72	7·93	—	—	—	0·41	—	—	—	0·02
29	155	703	2·93	63·78	24·13	11·64	—	—	—	0·45	—	—	—	0·11
33*	156	676	−1·61	88·76	8·21	3·03	—	0·01	—	—	—	—	0·01	0·02
34*	156	676	−1·77	68·97	18·45	10·61	—	1·93	—	—	—	0·05	—	0·00
35*	156	676	−1·98	45·46	33·94	16·38	—	4·19	—	—	—	0·04	—	0·02
36	155	678	3·97	99·25	—	—	—	—	—	0·63	—	0·10	0·02	0·82
37	155	678	3·89	40·75	40·90	17·90	—	—	—	0·01	—	0·45	0·01	0·31
41	152	700	2·78	63·37	20·14	11·47	4·96	—	—	—	—	0·05	—	0·14
42	140	786	3·71	55·08	29·35	14·82	—	—	—	0·65	—	0·09	—	0·44
43	140	786	3·48	55·41	28·70	15·07	—	—	—	0·82	—	—	—	0·85
38	155	678	3·78	9·47	62·41	27·28	0·01	—	—	0·35	—	0·49	0·01	0·97
45	57	737	−1·59	65·48	21·26	11·80	—	—	—	1·41	—	—	—	0·17
46	57	737	−1·87	59·80	25·27	14·64	—	—	—		—	—	—	0·09

Table 1: continued

	P (MPa)	*T* (°C)	ΔNNO[1]	gl	af	qtz	cpx	amph	fay	ox	bt/mdt	fl	chek/tit	r^2
47	151	661	−1·66	96·00	—	—	—	0·01	4·00	0·10	—	0·10	—	0·02
48	151	702	−1·94	51·32	29·35	15·75	—	3·59	—	—	—	—	—	0·05
50	151	702	−2·56	25·40	43·48	24·36	—	6·77	—	—	—	—	—	0·11
51	150	784	2·35	36·05	45·12	18·21	—	—	—	0·52	—	0·10	—	0·17
53*	52	686	−2·10	28·14	44·07	22·69	—	4·80	—	0·24	—	0·05	—	0·12
56	152	758	−3·13	56·36	26·16	17·41	—	—	—	—	—	0·07	—	1·84
57*	152	729	−3·20	45·19	34·17	19·51	—	1·00	—	—	—	0·12	—	0·00
58	152	773	−3·10	85·35	5·65	9·01	—	—	—	—	—	—	—	0·67
SMN49														
7	161	744	−1·13	97·91	—	2·08	—	—	—		—	—	—	0·00
9	148	703	−1·20	99·69	—	0·31	—	—	—		—	—	—	0·00
16	155	775	3·64	82·65	12·80	4·33	—	—	—		—	—	0·21	0·17
17	152	725	4·05	99·67	—	—	—	—	—	0·33	—	—	—	0·00
18	152	725	3·94	99·61	—	—	—	—	—	0·24	—	—	0·16	0·24
19	152	725	3·85	99·18	—	0·75	—	—	—	0·07	—	—	—	0·21
20	152	725	3·72	98·00	—	1·76	—	—	—	0·01	—	—	0·24	0·94
21	152	725	3·65	49·37	32·31	17·00	—	—	—	1·32	—	—	—	0·80
22	149	796	−1·79	99·99	—	0·01	—	—	—	—	—	—	—	0·00
23	149	796	−1·98	68·28	19·61	12·11	—	—	—	—	—	—	—	1·07
25	155	679	3·82	67·92	18·81	9·31	3·96	—	—	0·01	—	—	—	0·20
26	155	679	3·72	66·46	18·80	11·41	3·08	—	—	0·26	—	—	—	0·10
27	155	679	3·59	59·27	22·81	14·82	2·31	—	—	0·79	—	—	—	0·09
32	156	678	−1·59	71·62	19·42	8·95	—	0·01	—	—	—	—	0·01	0·28
33	156	678	−1·71	44·07	35·95	16·93	—	3·10	—	—	0·01	—	0·06	0·06
35	152	700	3·12	37·66	39·72	16·87	5·75	—	—	—	—	—	—	0·13
36	152	700	2·97	39·68	37·69	16·97	5·41	—	—	—	—	—	—	0·02
37	152	700	2·87	31·55	41·85	20·35	6·25	—	—	—	—	—	—	0·09
38	152	700	2·73	23·88	50·11	21·07	4·94	—	—	—	—	—	—	0·13
39	140	786	3·29	63·97	24·49	11·54	—	—	—	—	—	—	—	1·74
40	140	786	2·83	55·02	30·11	14·58	—	—	—	—	—	0·29	—	0·29
42	57	732	−1·56	85·12	9·94	4·94	—	—	—	—	—	—	—	0·88
43	57	732	−1·88	59·84	27·02	13·15	—	—	—	—	—	—	—	0·33
44	151	661	−1·66	98·29	—	—	—	—	—	—	1·44	0·24	0·04	0·21
45	151	702	−1·96	62·95	25·10	11·95	—	—	—	—	—	—	—	0·26
46	151	702	−2·14	46·06	34·54	18·67	—	—	—	0·74	—	—	—	—
48	150	784	2·16	14·57	59·29	21·57	4·39	—	—	0·01	—	0·28	—	0·03
52	150	731	—	98·29	—	1·22	—	—	—	—	0·49	—	—	0·00
53	150	731	—	61·00	25·98	11·99	—	—	—	—	1·03	—	—	0·30
54	150	731	0·09	11·61	57·72	24·14	—	6·28	—	—	—	0·26	—	0·17
55	52	679	−1·92	53·93	31·62	14·18	—	—	—	—	—	0·27	—	0·12
58	152	758	−3·13	52·03	31·74	15·99	—	—	—	—	—	0·24	—	0·21
59	152	729	−3·20	18·08	52·07	24·72	—	4·63	—	—	—	0·51	—	0·21
60	152	773	−3·10	65·92	20·09	13·99	—	—	—	—	—	—	—	1·27

gl, glass; af, alkali feldspar; qtz, quartz; cpx, clinopyroxene; amph, amphibole; fay, fayalite; ox, oxides; bt, biotite; montd, montdorite; fl, fluorite; chevk, chevkinite; tit, titanite.

*Charges where Ni contamination occurred. It should be noted that clinopyroxene was not reported in charge 002-21 by Scaillet & Macdonald (2001). Additional analyses confirmed this phase to be present, in agreement with the assemblages of neighbouring charges.

[1]$\Delta NNO = \log fO_2(\text{experiment}) - \log fO_2(NNO)$.

[2]Residual from mass balance calculations.

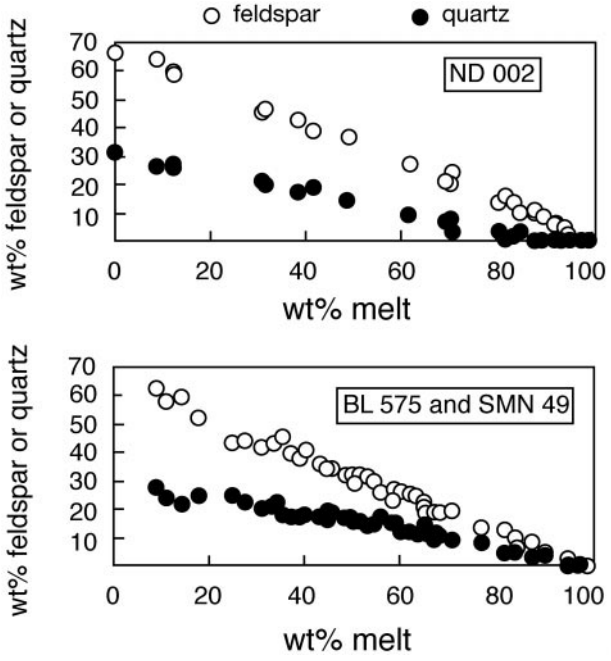

Fig. 3. Variation in the modal amount (wt %) of quartz and alkali feldspar with progressive crystallization in ND002, BL575 and SMN49 compositions. The wt % melt values are taken from Table 1. Error bars are smaller than symbol sizes.

for the three compositions over all their crystallization interval. Maximum abundances of minor phases in ND002 are 2·5 wt % clinopyroxene, 2·1 wt % fayalite, and 1·2 wt % oxide (Table 1). When present, biotite, amphibole, fluorite and a chevkinite-group mineral usually amount to <0·5 wt % each (Table 1). It should be noted that the calculated liquid fraction in charge 002-33, which yielded the most peralkaline melt composition from ND002, is below 1 wt %. In BL575 and SMN49, minor phases have the following maximum abundances (wt %); amphibole 6·8, clinopyroxene 4·5, biotite 1·4 and fluorite 0·5. When present, a chevkinite-group mineral, oxide and montdorite [a tetrasilicic mica, $(KFe^{2+}_{1.5}Mn^{2+}_{0.5}Mg_{0.5}\square_{0.5}Si_4O_{10}F_2)$] are <0·3 wt % each.

Feldspar

Representative compositions of feldspars are given in Table 2. Microprobe analyses were considered acceptable when the structural formulae fulfilled the following criteria: 7·98 < (Si + Al + Fe) < 8·02 and (Ca + Na + K) >1·9 (on a 16 oxygen basis). Only alkali feldspar precipitated from the melts in all but one charge, ND002-15, in which two plagioclase ($Ab_{50}An_{46}Or_3$) crystals were found). The plagioclase is too calcic to be in equilibrium with the coexisting alkali feldspar, suggesting that it represents either a local disequilibrium feature or a xenocryst present in the starting material. At T >700°C, the average feldspar composition of a given charge, calculated without taking into account the core composition of the large crystals discussed above, displays a standard deviation of <2 mol % in either Ab or Or components. We consider these average compositions as closely approaching equilibrium feldspar compositions (see also Carmichael & Mackenzie, 1963; Thompson & Mackenzie, 1967). For charges crystallizing two feldspars, we cannot assess to what extent the compositions listed in Table 2 represent equilibrium compositions.

At up to ~40% crystallization of the melt, the feldspars in ND002 show, under both reduced and oxidized conditions, a scatter of compositions between Or_{25} and Or_{57} (Fig. 4). This spread results from the effect of melt water content on feldspar composition, which varies with temperature under water-rich conditions, i.e. lower melt fraction at a given temperature. At ~780°C the feldspar reaches an Or content of 25–30 mol %, whereas below 700°C, it is Or_{57}. In contrast, at all temperatures, when the degree of crystallization increases (i.e. the melt water content decreases), the composition is constant, $Or_{40–45}$ (Fig. 4). At low fO_2 at both 150 and 50 MPa, anorthite contents reach a maximum of 2 mol % in near-liquidus and water-rich charges; Fe_2O_3 abundances range up to 0·7 wt %. At high fO_2 and 150 MPa, An reaches 4 mol % (except in the plagioclase-bearing charge) and Fe_2O_3 contents are up to 1 wt %.

Variations in feldspar composition in BL575 and SMN49 are less marked than in ND002, partly because the stability field of feldspar is smaller. Excluding charges possibly lying in the two-feldspar field and charge 49-16 whose feldspar is Or_{25}, all feldspar compositions are sodic sanidines in the range $Or_{34–42}$ (Fig. 4). CaO contents of feldspars in BL575 and SMN49 were barely detectable with the applied analytical conditions. All analyses show a substantial iron content, up to nearly 4 wt % under oxidizing conditions. There is no evidence on SEM images of oxide inclusions, suggesting that the iron is in solution in the feldspar.

Most feldspars in all three bulk compositions are peralkaline (Fig. 5), even when Fe is added to Al to counterbalance the alkalis. This compares to the situation in the natural phenocrysts (Macdonald *et al.*, 1987; Marshall, 1999). Alkali feldspar–melt relationships in the experiments are relatively simple. The melt is always more peralkaline than its coexisting feldspar (Fig. 5). In ND002, with one exception, feldspars are more potassic and more sodic than the coexisting melt (Fig. 5). This relationship closely matches that in the natural rock, ND002 being the only Olkaria comendite in which the feldspar phenocrysts are more sodic than

Table 2: Compositions of experimental feldspars (wt %)

Run:	002-3	002-4	002-5	002-7	002-9	002-11	002-15	002-16	002-18[1]	002-19	002-20	002-21	002-22	002-23
T/ΔNNO:[2]	788/−1·4	788/−1·4	788/−1.6	738/−1·1	699/−1·2	*794/−1·5*	794/4·1	794/3·9	752/4·2	752/4·1	752/3·9	752/3·9	788/−1·8	696/4·2
n:[3]	4	7	3	7	6	6	4	3	1	4	3	3	4	2
SiO_2	67·50(31)	67·83(127)	66·82(82)	67·31(24)	67·01(55)	67·31(106)	67·22(105)	67·37(51)	67·85	68·04(60)	67·82(36)	68·41(31)	67·86(46)	66·43(17)
Al_2O_3	18·40(20)	17·99(33)	17·65(60)	18·44(16)	18·25(32)	17·77(52)	18·73(49)	19·40(64)	18·97	18·73(16)	18·64(21)	17·60(38)	18·61(33)	17·85(6)
Fe_2O_3[4]	0·32(10)	0·35(12)	0·59(8)	0·35(14)	0·38(11)	0·24(10)	0·21(9)	0·20(10)	0·22	0·22(4)	0·70(34)	0·85(12)	0·21(6)	0·27(13)
CaO	0·22(3)	0·14(2)	0·16(2)	0·11(5)	0·08(5)	0·28(10)	0·30(2)	0·79(46)	0·13	0·20(2)	0·21(4)	0·15(10)	0·11(10)	0·15(8)
Na_2O	7·22(26)	6·82(19)	6·45(23)	6·45(39)	5·95(24)	7·71(31)	7·22(13)	8·26(63)	6·60	7·04(25)	6·79(10)	6·40(32)	7·30(14)	4·99(18)
K_2O	6·10(25)	6·67(35)	6·93(12)	7·12(41)	8·06(41)	5·14(29)	6·44(31)	4·45(129)	6·91	6·53(41)	7·11(22)	6·94(12)	6·66(24)	9·67(49)
Total	99·75	99·80	98·60	99·78	99·73	98·43	100·12	100·47	100·69	100·75	101·27	100·34	100·75	99·36
Ab	63·6(14)	60·4(18)	58·1(7)	57·6(26)	52·7(21)	68·6(7)	62·1(14)	71·0(52)	58·8	61·5(20)	58·6(5)	57·9(12)	62·2(12)	43·6(20)
An	1·1(2)	0·7(1)	0·8(1)	0·6(2)	0·4(3)	1·4(5)	1·4(1)	3·8(22)	0·7	1·0(1)	1·0(2)	0·8(4)	0·5(5)	0·7(4)
Or	35·3(15)	38·9(18)	41·1(7)	41·8(27)	47·0(2)	30·0(9)	36·5(14)	25·2(73)	40·5	37·5(19)	40·4(7)	41·4(16)	37·3(13)	55·7(24)
Run:	002-24	002-25	002-26	002-28	002-29	002-30	*002-31*	*002-33*	002-34	002-35	002-37	002-37	002-38	002-39[5]
T/ΔNNO:	696/4·1	696/3·9	696/2·9	*790/−1·8*	*790/−1·9*	*790/−2·1*	693/−1·6	693/−1·8	*756/−1·4*	*756/−1·5*	661/−1·7	661/−1·7	784/2·4	*688/−2·1*
n:	6	5	5	2	1	3	4	5	8	8	1	1	1	3
SiO_2	67·31(14)	65·95(52)	65·68(70)	67·46(9)	69·55	67·99(67)	67·37(130)	67·62(37)	66·59(43)	66·40(64)	67·39	65·67	68·32	68·61(16)
Al_2O_3	17·73(60)	17·77(11)	17·58(25)	17·85(90)	17·46	17·91(25)	18·48(47)	18·47(34)	18·80(29)	18·23(25)	18·99	18·39	17·38	18·00(17)
Fe_2O_3	0·46(27)	0·92(18)	0·71(13)	0·46(2)	0·22	0·26(12)	0·49(11)	0·55(17)	0·40(21)	0·41(12)	0·39	0·27	0·99	0·56(13)
CaO	0·14(6)	0·02(3)	0·01(1)	0·33(12)	0·11	0·08(4)	0·04(2)	0·01(1)	0·24(15)	0·06(4)	0·03	0·00	0·10	0·00
Na_2O	6·07(43)	6·54(11)	6·31(24)	7·09(40)	7·20	6·98(15)	6·81(34)	6·48(9)	6·94(23)	6·40(24)	7·27	5·52	6·60	6·62(13)
K_2O	7·80(73)	7·16(35)	7·24(7)	5·62(13)	5·93	6·77(11)	7·28(19)	7·50(24)	6·42(26)	7·01(35)	5·89	9·12	6·69	6·89(33)
Total	99·50	98·35	97·53	98·80	100·46	99·98	100·47	100·63	99·40	98·51	99·95	98·97	100·08	100·68
Ab	53·8(37)	58·1(12)	56·9(11)	64·6(12)	64·5	60·8(9)	58·6(17)	56·7(10)	61·4(15)	57·9(19)	65·1	47·9	59·7	59·3(15)
An	0·7(3)	0·1(2)	0·0(0)	1·7(7)	0·5	0·4(2)	0·2(1)	0·0(1)	1·2(7)	0·3(2)	0·1	0·0	0·5	0·0
Or	45·5(40)	41·8(12)	43·0(11)	33·7(5)	35·0	38·8(7)	41·2(18)	43·2(10)	37·4(16)	41·8(20)	34·7	52·1	39·8	40·7(15)

Run:	002-42	002-43	002-44	575-23	575-24	575-27	575-28	575-29	575-33	575-33	575-34	575-35	575-35	575-37
T/ΔNNO:	758/−3·1	729/−3·2	773/−3·1	791/−2·1	791/−2·3	703/3·2	703/3·0	703/2·9	676/−1·6	676/−1·6	676/−1·8	676/−1·9	676/−1·9	678/3·9
n:	6	4	4	5	8	14	17	11	1	1	6	1	1	1
SiO_2	67·14(67)	66·75(103)	66·38(35)	67·37(57)	67·42(76)	65·69(59)	67·27(92)	65·76(57)	67·30	66·98	67·44(27)	68·39	67·97	67·72
Al_2O_3	18·21(37)	17·64(31)	18·26(16)	18·26(40)	18·31(15)	17·18(53)	17·11(58)	16·70(83)	18·53	18·05	18·29(36)	17·28	18·06	18·28
Fe_2O_3	0·40(15)	0·67(4)	0·35(4)	0·87(12)	0·76(16)	1·72(22)	1·87(51)	2·03(76)	0·86	0·90	0·84(12)	0·81	1·42	0·98
CaO	0·07(15)	0·01(1)	0·05(1)	0·00	0·00	0·00(1)	0·00	0·00	0·00	0·00	0·00	0·00	0·00	0·00
Na_2O	6·61(21)	6·47(17)	6·75(5)	6·94(18)	7·33(34)	7·09(31)	6·80(27)	6·82(33)	6·78	6·40	6·39(17)	5·89	7·07	7·12
K_2O	7·15(28)	7·22(32)	7·28(13)	6·74(39)	6·66(38)	6·29(38)	6·43(38)	6·43(27)	6·92	7·93	7·63(26)	7·92	6·91	7·09
Total	99·58	98·75	99·07	100·19	100·49	97·97	99·49	97·74	100·40	100·25	100·59	100·28	101·43	101·19
Ab	58·2(16)	57·7(15)	58·3(3)	61·0(15)	62·6(21)	63·2(17)	61·7(15)	61·7(17)	59·82	55·09	56·0(10)	53·1	60·8	60·45
An	0·3(7)	0·0	0·2(1)	0·0	0·0	0·0	0·0	0·0	0·00	0·00	0·0	0·0	0·0	0·00
Or	41·4(18)	42·3(15)	41·4(4)	39·0(15)	37·4(21)	36·8(17)	38·3(15)	38·3(17)	40·18	44·91	44·0(10)	46·9	39·2	39·55
Run:	575-37	575-38	575-38	575-45	575-46	*575-48*	*575-51*	575-53	575-54	575-56	575-57	575-58	49-16	49-21
T/ΔNNO:	678/3·9	678/3·8	678/3·8	*737/−1·6*	*737/−1·9*	702/−1·9	784/2·4	*686/−2·1*	*686/−2·3*	758/−3·1	729/−3·2	773/−3·1	775/3·6	725/3·7
n:	1	1	1	7	5	1	8	5	1	9	1	7	5	2
SiO_2	66·99	68·10	68·21	66·60(104)	66·50(37)	65·53	68·17(49)	68·49(28)	68·72	68·38(99)	67·17	67·24(106)	67·92(74)	66·11(34)
Al_2O_3	18·34	17·75	17·29	17·78(37)	17·99(43)	17·92	15·75(93)	17·69(41)	18·13	17·51(70)	18·34	17·51(57)	17·60(56)	17·53(53)
Fe_2O_3	1·07	2·07	2·27	1·02(27)	0·99(17)	0·79	3·35(49)	1·33(46)	1·00	0·97(28)	1·07	0·90(9)	1·28(42)	0·66(3)
CaO	0·00	0·00	0·00	0·00	0·01(2)	0·00	0·00	0·00	0·00	0·00	0·00	0·00	0·01(1)	0·00
Na_2O	6·07	6·64	7·16	6·99(15)	6·80(23)	6·90	7·23(20)	6·86(27)	7·29	6·90(23)	6·79	6·80(18)	8·24(21)	6·80(10)
K_2O	7·90	7·61	6·03	6·25(19)	6·85(26)	6·76	5·91(31)	6·67(29)	6·18	6·43(38)	7·22	6·87(32)	4·31(30)	6·78(6)
Total	100·37	102·16	100·95	98·64	99·15	97·89	100·42	101·03	101·31	100·19	100·59	99·32	99·35	97·88
Ab	53·87	57·0	64·3	63·0(11)	60·1(15)	60·8	65·0(11)	61·0(19)	64·2	62·0(17)	58·8	60·1(8)	74·4(16)	60·4(2)
An	0	0·0	0·0	0·0	0·0(1)	0·0	0·0	0·0	0·0	0·0	0·0	0·0	0·0	0·0
Or	46·13	43·0	35·7	37·0(11)	39·9(15)	39·2	35·0(11)	39·0(19)	35·8	38·0(17)	41·2	39·9(8)	25·6(16)	39·6(2)

Table 2: continued

Run:	49-23	49-25	49-25	49-26	49-26	49-27	49-27	49-32	49-32	49-33	49-34	49-34	49-42	49-43
T/ΔNNO:	796/−1·9	679/3·8	679/3·8	679/3·7	679/3·9	679/3·6	679/3·6	678/−1·6	678/−1·6	678/−1·7	678/−2·0	678/−2·0	*732/−1·6*	*732/−1·9*
n:	7	1	1	1	1	1	1	1	1	4	1	1	4	3
SiO_2	67·46(68)	67·02	66·53	66·01	64·94	65·61	66·19	68·67	68·16	67·52(62)	67·04	68·10	67·13(59)	66·73(57)
Al_2O_3	17·83(58)	17·76	17·98	17·01	16·33	16·75	16·38	17·62	18·40	17·72(69)	18·00	17·77	18·57(21)	18·03(6)
Fe_2O_3	1·03(56)	1·07	0·81	2·63	3·25	2·57	3·01	1·72	0·90	1·43(38)	1·50	1·34	0·96(27)	1·25(25)
CaO	0·00	0·00	0·00	0·00	0·00	0·00	0·00	0·01	0·00	0·03(7)	0·00	0·00	0·00	0·00
Na_2O	7·09(29)	7·59	6·47	6·86	6·80	6·22	7·20	7·74	6·48	6·80(31)	6·80	7·88	7·54(22)	7·20(15)
K_2O	6·51(40)	5·82	7·30	6·97	6·25	7·52	6·51	5·95	7·62	7·17(21)	7·07	5·77	5·91(37)	6·38(10)
Total	99·93	99·27	99·08	99·47	97·57	98·67	99·29	101·70	101·56	100·67	100·40	100·86	100·11	99·59
Ab	62·3(24)	66·4	57·4	59·9	62·3	55·7	62·7	66·4	56·4	58·9(13)	59·4	67·5	66·0(18)	63·2(8)
An	0·0	0·0	0·0	0·0	0·0	0·0	0·0	0·1	0·0	0·2(3)	0·0	0·0	0·0	0·0
Or	37·7(24)	33·6	42·6	40·1	37·7	44·3	37·3	33·6	43·6	40·9(16)	40·6	32·5	34·0(18)	36·8(8)

Run:	49-45	49-46	49-47	49-48	49-53	49-54	49-55	49-57	49-58	49-59	49-60
T/ΔNNO:	702/−1·9	702/−2·1	702/−2·7	784/2·2	731/n.d.[6]	731/0·1	*679/−1·9*	*679/−2·4*	758/−3·1	729/−3·2	773/−3·1
n:	7	1	5	10	3	10	10	1	8	6	6
SiO_2	67·70(63)	66·63	66·90(36)	67·36(77)	67·74(182)	67·43(154)	68·31(71)	66·91	67·13(51)	66·90(29)	67·13(20)
Al_2O_3	17·49(51)	17·83	17·57(59)	15·82(110)	17·47(62)	16·55(62)	17·60(50)	17·29	17·30(50)	17·30(42)	17·91(26)
Fe_2O_3	1·34(37)	1·39	1·13(63)	2·95(133)	1·23(78)	2·10(70)	1·06(34)	1·87	1·40(21)	1·38(30)	0·87(20)
CaO	0·00	0·00	0·01(1)	0·01(1)	0·00	0·01(1)	0·00	0·02	0·00	0·00	0·00
Na_2O	6·84(25)	6·67	6·38(22)	6·91(20)	7·19(20)	6·66(27)	6·70(35)	6·55	6·98(15)	6·74(12)	7·02(11)
K_2O	6·69(52)	7·29	7·37(43)	6·04(17)	6·16(41)	6·65(31)	7·07(46)	7·45	6·45(16)	6·94(29)	6·79(27)
Total	100·07	99·80	99·36	99·09	99·79	99·40	100·73	100·09	99·27	99·26	99·72
Ab	60·8(24)	58·2	56·8(21)	63·4(8)	64·0(21)	60·3(18)	59·0(25)	57·1	62·2(6)	59·6(12)	61·1(12)
An	0·0	0·0	0·0	0·1(1)	0·0	0·0	0·0	0·1	0·0	0·0	0·0
Or	39·1(24)	41·8	43·2(22)	36·5(8)	36·0(21)	39·7(18)	41·0(25)	42·8	37·8(6)	40·4(12)	38·9(12)

Numbers in parentheses indicate one standard deviation of replicate analyses in terms of smallest units cited.
[1]Inherited feldspar.
[2]Temperature (°C)/fO_2 (given relative to NNO) conditions of the charge. Italicized numbers are for a pressure of 50 MPa, all others for 150 MPa.
[3]Number of analyses.
[4]Total Fe as Fe_2O_3.
[5]Feldspar not reported by Scaillet & Macdonald (2001).
[6]n.d., not determined.

JOURNAL OF PETROLOGY VOLUME 44 NUMBER 10 OCTOBER 2003

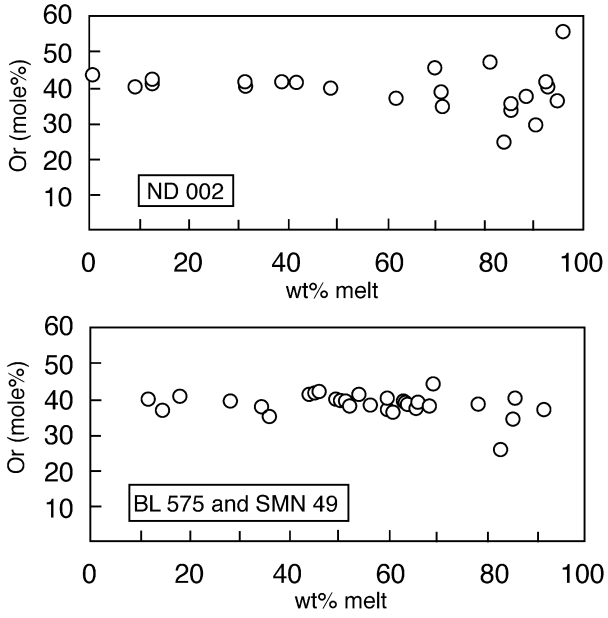

Fig. 4. Variation in alkali feldspar compositions (as mol % Or) with progressive crystallization in the ND002, BL575 and SMN49 compositions. At melt proportions <60 wt %, all feldspars have constant composition of *c*. Or_{40}. Error bar equals the size of the symbols.

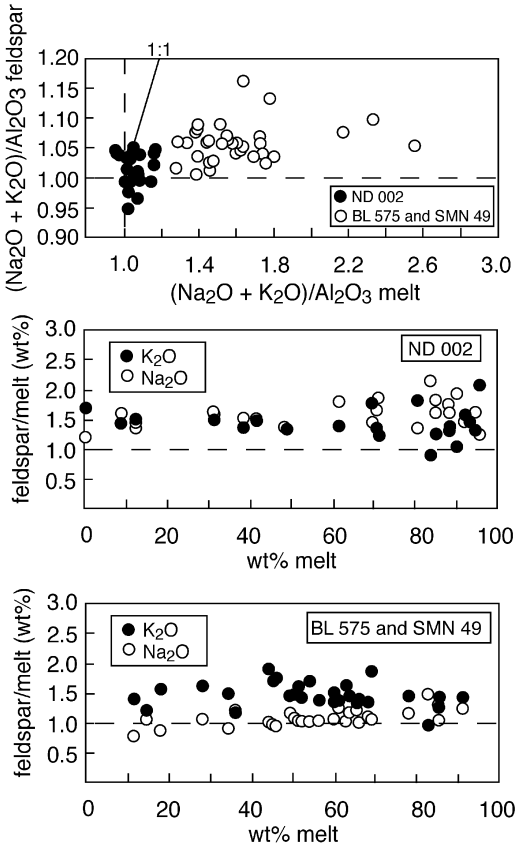

Fig. 5. Feldspar–melt relationships. (a) With few exceptions, mainly from oxidized runs from ND002, feldspars are peralkaline (NK/A>1) but they are always less so than coexisting melt. (b) Evolution of the alkali ratio between melt and coexisting feldspar with progressive crystallization in ND002 charges. Feldspar is always both more potassic and sodic than coexisting melt. (c) Evolution of the alkali ratio between melt and coexisting feldspar with progressive crystallization in BL575 and SMN49 charges. At low melt fraction, feldspar can be less sodic than coexisting melt. Error bars are equal to, or smaller than, the size of the symbols.

the coexisting glass. In BL575 and SMN49, feldspars are, with one exception, more potassic than coexisting glass (Fig. 5). In contrast, the Na_2O contents of feldspar and melt are similar up to 40 wt % crystallization. Beyond, the melt becomes richer in Na_2O than the feldspar.

Clinopyroxene

Clinopyroxene is present in almost all runs of ND002, in only four higher fO_2 runs of BL575 and in nine higher fO_2 runs of SMN49. Representative analyses are listed in Table 3. Several problems hampered the determination of clinopyroxene composition in ND002 charges. First, it was difficult to distinguish between phenocrysts and newly crystallized minerals. Second, the generally small size of crystals (<5 μm) makes it very difficult to obtain analyses free of glass contamination, as revealed by the elevated K_2O content of many analyses (Table 3). Thus, although identifying clinopyroxene in ND002 was not a problem, we could not obtain high-quality clinopyroxene analyses in most charges.

One criterion used to distinguish between the pyroxenes in ND002 was Al_2O_3 content, which is often higher in experimentally derived minerals (>1 wt %; see also Dall'Agnol *et al.*, 1999) than in their low-pressure natural counterparts (<0·5 wt % in Olkaria rocks; Macdonald *et al.*, 1987). Glass contamination is marked by a combination of elevated values of Al_2O_3, Na_2O and K_2O contents. Analyses in which either elevated Al_2O_3 or Na_2O content occurs alone, or is not associated with high K_2O, are thus considered to reflect a true compositional feature of the clinopyroxenes.

Clinopyroxenes in ND002 runs range from ferrosalite to ferroaugite. In high fO_2 runs at 150 MPa, they become slightly more calcic and less Fe rich as the proportion of melt decreases. In reduced runs, no such trend is apparent because clinopyroxene breaks down when approaching the solidus (Scaillet & Macdonald, 2001). At 150 MPa, the clinopyroxene in reduced runs is significantly more Fe rich than that in the more oxidized runs, with X_{Fe} 69–79 and 25–47, respectively (Table 3). Even so, the pyroxenes synthesized at low fO_2 are distinctly more magnesian than the phenocrysts in ND002 (X_{Fe} 0·88; Marshall, 1999), possibly because the experimental redox conditions were slightly more oxidizing than those prevailing

Table 3: Compositions of experimental pyroxenes (wt %)

Run:	002-4	002-5	002-6	002-15	002-16	002-18	002-18	002-19	002-23	002-28	002-30	49-25	49-27	49-48
T/ΔNNO:[1]	788/−1·4	788/−1·6	738/−1·1	794/4·1	794/3·9	752/4·2	752/4·2	752/4·1	696/4·2	*790/−1·8*	*790/−2·1*	679/3·8	679/3·6	784/2·2
						bd[2]	bd							
n:[3]	1	1	4	3	1	1	1	1	1	2	1	1	3	6
SiO_2	52·10	54·68	52·28(195)	51·37(220)	45·78	52·53	50·43	45·47	51·71	53·28(20)	53·02	49·70	52·15(75)	52·03(63)
TiO_2	0·20	0·32	0·19(5)	0·77(106)	4·35	0·16	1·96	3·94	1·08	0·13(1)	1·13	1·30	1·15(76)	1·35(30)
Al_2O_3	2·00	3·62	1·47(87)	1·95(24)	5·65	1·54	2·83	6·15	3·02	0·87(7)	2·49	0·65	0·50(34)	1·12(44)
FeO[4]	23·56	21·77	19·42(197)	9·33(11)	7·90	14·93	7·39	7·66	8·89	10·31(20)	8·45	30·62	29·24(87)	28·44(115)
MgO	3·24	2·54	4·92(74)	10·69(45)	11·04	9·07	12·44	11·31	10·24	13·57(18)	12·06	0·28	0·08(2)	0·06(2)
MnO	0·64	0·51	0·00	0·56(19)	0·03	0·78	0·27	0·03	0·44	0·43(12)	0·02	0·09	0·19(6)	0·07(7)
CaO	15·81	13·48	18·72(95)	20·19(62)	22·70	18·54	22·02	22·56	19·80	20·03(22)	20·66	0·58	0·32(13)	0·22(3)
Na_2O	0·96	1·68	0·99(29)	1·62(15)	0·96	2·60	0·84	0·88	3·07	0·31(11)	0·88	12·92	13·13(52)	12·04(53)
K_2O	0·73	1·26	0·42(23)	0·32(5)	0·12	0·27	0·11	0·15	0·53	0·12(3)	0·29	0·07	0·02(2)	0·22(13)
Total	99·24	99·85	98·42	96·81	98·52	100·41	98·29	98·14	98·78	99·04	98·99	96·21	96·77	95·55
En%	11·66	10·39	16·8(17)	35·1(13)	34·73	29·46	38·37	35·53	34·74	40·2(0)	38·09	—	—	—
Fs%	47·51	49·97	37·2(26)	17·2(1)	13·93	27·22	12·79	13·51	16·93	17·1(0)	14·98	—	—	—
Wo%	40·83	39·64	45·9(17)	47·7(13)	51·34	43·32	48·84	50·96	48·32	42·6(0)	46·92	—	—	—
XFe[5]	0·79	0·81	0·69	0·32	0·29	0·47	0·25	0·28	0·32	0·30	0·28	0·98	0·99	0·99

Numbers in parentheses indicate one standard deviation of replicate analyses in terms of smallest units cited.
[1]Temperature (°C)/fO_2 (given relative to NNO) conditions of the charge. Italicized numbers are for a pressure of 50 MPa, all others for 150 MPa.
[2]bd, analysis from breakdown products of a former pyroxene phenocryst.
[3]Number of analyses.
[4]Total Fe as FeO.
[5]XFe = Fe/(Fe + Mn + Mg), in moles.

during phenocryst crystallization. All clinopyroxenes in ND002 runs have relatively modest Na contents, which increase either as the melt H_2O content decreases, or as the amount of crystallization increases. The trend, however, is obscured by glass contamination, as shown in high K_2O contents (Table 3). However, the maximum observed Na_2O content is 3·08 wt % at 696°C, H_2O saturation and high fO_2 (Table 1, charge 002-23). At high fO_2, clinopyroxene in ND002 may be either peraluminous (high T) or peralkaline (low T), not taking into account the CaO content. At low fO_2 at 150 MPa, it is always slightly peralkaline. Thus ND002 may crystallize a calcic clinopyroxene that has higher NK/A than the coexisting liquid. We noted above the generally elevated Al contents of the synthetic pyroxenes; these contents are significantly higher at high fO_2 than at low fO_2, perhaps suggesting a coupled substitution of the type Al Fe^{3+} for $Fe^{2+}Si$.

Clinopyroxenes in BL575 and SMN49 are all nearly end-member aegirine, with low to extremely low MgO and CaO contents (Table 3). TiO_2 is constant at about 1 wt %; Al_2O_3 content is more variable but barely exceeds 1 wt %. Analysed minerals do not display any systematic compositional changes with variations in temperature and melt H_2O contents.

Amphibole

Representative amphibole analyses are listed in Table 4. Amphiboles crystallizing from ND002 were difficult to analyse as this phase mainly occurs in extensively crystallized charges, or even below the solidus, and most analyses display substantial contamination by neighbouring phases, as revealed by grossly non-stoichiometric structural formulae. In contrast, in BL575 and SMN49 all amphibole analyses in a given charge are identical within analytical uncertainty. The sole exception is when Ni contamination arises, in which case the amphibole analyses of a given charge can display NiO varying from 0 to 4·55 wt %. Comparison of contaminated and uncontaminated analyses suggests that Ni substitutes for Fe.

Amphibole structural formulae were calculated using the assumption that the sum of cations other than Ca, Na and K is equal to 13, because that is known to yield Fe^{3+}/Fe^{2+} estimates that best approximate those determined by wet chemistry (e.g. Hawthorne, 1976; Enders *et al.*, 2000). Amphibole names were determined following Leake *et al.* (1997). Amphibole crystallizing above the solidus in ND002 (two charges only) is ferro-richterite; under sub-solidus conditions, it is either katophorite (charge 31, Table 4) or arfvedsonite (charge 40, Table 4). Overall, although the relatively restricted stability field of amphibole in ND002 makes it difficult to evaluate the effect of P, T and melt H_2O variations on amphibole composition, the occurrence of sodic–calcic amphibole above the solidus and of sodic amphibole below it suggests that a fall in T or decrease in aH_2O drives amphibole compositions from sodic–calcic to sodic. Such a trend is in line with an increase in the Na_2O content of residual liquids as crystallization proceeds under low fO_2 conditions (see below). Amphibole does not occur as a phenocryst phase in the natural rock ND002, which is consistent with its relatively late crystallization in the experiments.

Amphibole crystallizing in BL575 and SMN49 is exclusively arfvedsonite. It has Fe/(Fe + Mg) >0·97, and MnO > MgO (Table 4). The compositions closely match those of amphiboles found as phenocrysts in the Olkaria comendites (Macdonald *et al.*, 1987). Variations of amphibole composition with P, T and melt H_2O content are as follows: at fixed P and T, a decrease in melt H_2O content decreases the CaO content, from nearly 2·5 wt % at H_2O saturation, 660°C and 150 MPa, to 0·15 wt % near the solidus (Table 4, Fig. 6a). The decrease is linear between 6 and 3 wt % H_2O in the melt and flattens out at lower H_2O. This decrease is usually accompanied by an increase in Na_2O content of the amphibole. Thus, variations in melt H_2O contents from near-saturation to dry conditions drive amphibole from sodic–calcic toward sodic compositions. Al_2O_3 and K_2O (not shown) abundances seem insensitive to variations in temperature and melt H_2O content (Fig. 6a), whereas a decrease in pressure appears to lead to a decrease in Al_2O_3 (and K_2O, not shown; Fig. 6b). A decrease in melt H_2O content is also marked by a progressive increase in the F content of amphibole (Fig. 6a), from 2 to nearly 4 wt % in the most heavily crystallized, amphibole-bearing charges (Table 4). This increase in F content mirrors that in the liquid (Fig. 6c). The partitioning of F between amphibole and melt decreases from about 2·7 to 1 as the F content of the amphibole increases from 2 to >3 wt %. Amphibole remains remarkably poor in Cl, even when the coexisting liquids reach Cl contents close to 1 wt % (see below), a point noted for the natural phenocrysts by Macdonald *et al.* (1987).

Fe–Ti oxides

Representative analyses of Fe–Ti oxides are listed in Table 5. In ND002, under reducing conditions, only ilmenite is present; the very small crystal size makes it difficult to obtain reliable analyses. In uncontaminated mineral analyses, the ilmenite content is 97 mol %. Under oxidizing conditions, only haematite is present, with ilmenite <10 mol % (Table 5). In the more peralkaline samples, the oxide was satisfactorily analysed

Table 4: Compositions of experimental amphiboles (wt %)

Run:	002-31	002-40[1]	002-44[1]	575-47	49-32	49-33	49-34	49-47	49-54	49-56	49-57	49-59
T/ΔNNO:[2]	693/−1·6	*688/−2·1*	773/−3·1	661/−1·7	678/−1·6	678/−1·7	678/−2·0	702/−2·7	731/0·1	*679/−2·1*	*679/−2·4*	729/−3·2
n:[3]	1	1	1	2	5	5	3	4	5	6	5	5
SiO_2	46·34	49·49	46·54	48·29(63)	48·36(29)	49·63(102)	50·62(122)	50·86(124)	51·27(41)	49·61(59)	50·02(95)	49·79(83)
TiO_2	1·02	0·56	1·32	0·79(10)	0·87(13)	0·96(10)	1·00(7)	0·85(13)	0·83(8)	0·84(12)	1·06(24)	0·94(23)
Al_2O_3	2·72	2·06	3·0	1·40(26)	0·92(6)	0·99(32)	1·42(52)	1·69(50)	1·74(25)	1·00(27)	0·68(11)	1·42(68)
FeO_{tot}[4]	32·65	32·61	22·25	33·07(47)	37·41(27)	35·72(89)	34·22(77)	34·05(58)	30·43(73)	35·01(64)	34·94(48)	33·64(114)
MgO	2·77	1·98	6·67	0·77(7)	0·66(8)	0·37(3)	0·25(5)	0·34(1)	0·31(2)	0·44(4)	0·34(12)	0·53(14)
MnO	1·31	2·02	0·53	0·66(11)	0·79(7)	0·68(16)	0·53(6)	0·54(5)	0·62(7)	0·53(10)	0·58(6)	0·51(7)
CaO	6·84	0·79	9·45	2·48(16)	1·44(13)	0·79(5)	0·40(6)	0·30(3)	0·20(4)	0·54(5)	0·38(5)	0·43(6)
Na_2O	3·30	6·33	3·16	5·90(15)	6·70(13)	7·79(39)	7·97(18)	7·52(32)	8·66(28)	7·63(29)	7·93(18)	7·92(18)
K_2O	0·72	1·32	1·02	0·90(9)	0·84(11)	1·07(19)	1·53(27)	1·52(16)	1·54(16)	1·09(6)	1·07(12)	1·37(20)
F	1·78	3·61	2·97	1·93(21)	2·48(17)	2·72(13)	2·99(6)	3·47(8)	3·65(12)	3·25(18)	3·47(19)	3·67(23)
Cl	0·08	0·06	0·18	0·04(4)	0·02(2)	0·02(2)	0·03(2)	0·05(2)	0·05(3)	0·03(4)	0·04(2)	0·02(4)
F=O	0·75	1·52	1·25	0·81	1·04	1·15	1·26	1·46	1·54	1·37	1·46	1·54
Total	98·77	99·30	95·64	95·40	99·45	99·59	99·70	99·72	97·75	98·59	99·06	98·71
XFe[5]	0·84	0·85	0·64	0·94	0·95	0·96	0·97	0·97	0·96	0·96	0·97	0·96

Numbers in parentheses indicate one standard deviation of replicate analyses in terms of smallest units cited.
[1]Also contains NiO: 0·71 wt % (002-40) and 1·66 wt % (002-44).
[2]Temperature (°C)/fO_2 (given relative to NNO) conditions of the charge. Italicized numbers are for a pressure of 50 MPa, all others for 150 MPa.
[3]Number of analyses.
[4]Total Fe as FeO.
[5]$X\text{Fe} = \text{Fe}/(\text{Fe} + \text{Mn} + \text{Mg})$, in moles.

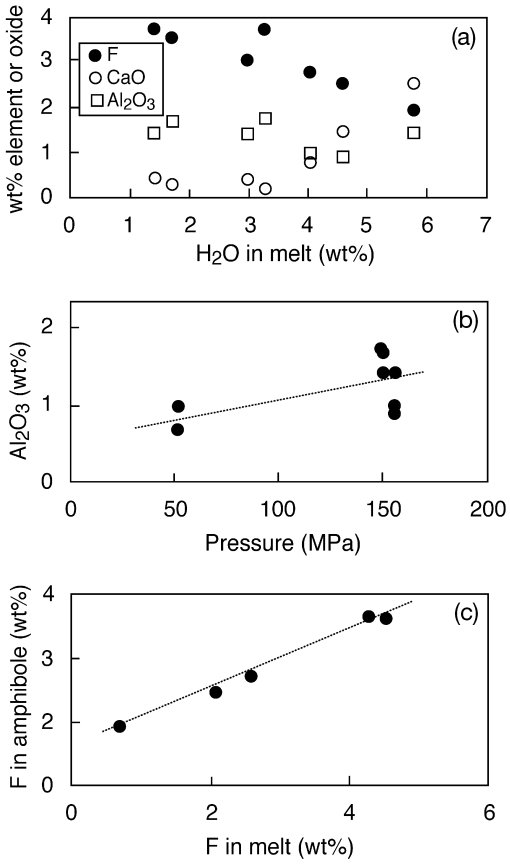

Fig. 6. Variation of amphibole composition in SMN49. (a) Al_2O_3, CaO and F vs H_2O in melt. (b) Al_2O_3 vs pressure. (c) F vs F in melt. Error bars are smaller than the size of the symbols.

only in SMN49, and under high fO_2 only (no oxide field could be defined at low fO_2; Scaillet & Macdonald, 2001). It is mostly haematite with low to very low ilmenite content (Table 5). In charge 49-20, magnetite close to the end-member composition crystallized in addition to haematite. Its ulvöspinel content is also very low.

Altogether, the extremely Ti-poor nature of the coexisting oxides shows that the prevailing fO_2 of these more oxidizing runs is close to the haematite–magnetite (HM) buffer curve, in agreement with the NNO + 4 value obtained from H_2-sensor measurements on similar runs (Scaillet & Macdonald, 2001). The coexistence of the two oxides in this charge shows that, under certain extreme conditions, mildly peralkaline melts may crystallize two oxides. No two-oxide comendites have yet been found at Olkaria, which again suggests that the natural redox conditions were more reducing.

Other phases

Representative analyses of fayalite, biotite, montdorite, a chevkinite-group mineral and titanite are listed in Table 6. Fayalite is present only in ND002 and has been analysed in near-solidus charges. X_{Fe} exceeds 0·90 and the elevated MnO contents, often seen in peralkaline silicic rocks (e.g. Carmichael, 1962), seem to decrease with rise in temperature (Table 6). The few biotites analysed in ND002 have high FeO contents, with <3 wt % MgO. They are rich in TiO_2 and F (up to 3·4 wt %); Cl contents are $<0{\cdot}5$ wt %. Biotites in both BL575 and SMN49 are even more Fe rich (FeO* close to 40 wt %), with MgO contents <1 wt %. TiO_2 contents are slightly lower than in ND002, with F contents *c.* 2 wt % (Table 6). The biotite–melt partition coefficient varies from 2·2 to 2·7 for F and from 0·3 to 0·8 for Cl.

Montdorite was first described by Robert & Maury (1979) in a comendite sill from the French Massif Central and subsequently reported from mildly peralkaline silicic rocks of the Questa caldera, New Mexico, by Czamanske & Dillet (1988). The only montdorite occurrence in the Olkaria run products (charge 49-33, Table 6) has an F content of nearly 8 wt %, accompanying very low amounts of Al_2O_3. The analysis is close to the expected end-member composition. Biotite phenocrysts occur at Olkaria in some moderately peralkaline rocks, including SMN49. Although they are not tetrasilicic micas, Macdonald *et al.* (1987) noted that they are poor in Al, having insufficient to fill, with Si, the tetrahedral sites.

Partial analyses of a chevkinite-group [$(Ce,La,Ca)_4(Fe^{2+},Mg)_2(Ti,Fe^{3+})_3Si_4O_{22}$] mineral were obtained mostly in high fO_2 charges, where it forms larger grains. CaO varies from >5 to 0·9 wt % (Table 6), being higher in ND002 than in BL575 and SMN49, reflecting the natural occurrences in Olkaria rocks and the bulk composition of the host rocks (Macdonald *et al.*, 2002). Analyses from SMN49 suggest, however, that part of this CaO variation is due to increase with rise in temperature. The F content is constant at around 1 wt %, as is the FeO content, which seems to be unaffected by changes in fO_2 [compare charges 49-24 (oxidized) and 49-44 (reduced)]. In contrast, the TiO_2 content shows substantial variation that cannot be correlated with any experimental parameter, although the variation could partly reflect mixes of inherited phenocrysts and newly grown crystals. A Ti–Ca- and Si-rich phase, probably titanite, was frequently present in charges 002, but under oxidized conditions only (Table 6).

Glass

The glass compositions in significantly crystallized charges are listed in Table 7; all glass data are plotted in relevant figures. Glass compositions in near- or above-liquidus charges are always close to the starting

Table 5: Compositions of experimental Fe–Ti oxides (wt %)

Run:	002-10	002-16	002-17	002-18	49-17	49-20	49-20	49-48	49-52	49-53
T/ΔNNO:[1]	*794/−1·5*	794/3·9	752/4·3	752/4·2	725/4·1	725/3·7	725/3·7	784/2·2	731/n.d.[2]	731/n.d.
n:[3]	1	1	1	1	2	1	1	3	2	2
TiO_2	47·17	3·97	6·27	4·85	5·46(37)	0·34	6·22	5·60(117)	0·95(17)	1·11(6)
Al_2O_3	0·04	0·20	0·13	0·60	0·03(2)	0·00	0·00	0·00(0)	0·02(1)	0·00(3)
Fe_2O_3	3·77	93·19	87·38	91·12	88·27520)	68·54	86·98	86·40(27)	98·77(9)	98·34(72)
FeO[4]	40·20	2·02	4·66	3·71	4·66(21)	29·15	5·44	4·94(98)	0·10(14)	0·32(23)
MgO	0·64	0·67	0·32	0·30	0·01(2)	0·14	0·01	0·00(0)	0·02(3)	0·05(7)
MnO	1·07	0·35	0·41	0·12	0·23(9)	2·05	0·14	0·10(7)	0·71(6)	0·58(15)
Total	92·90	100·40	99·17	100·71	98·66	100·21	98·79	97·04	100·57	100·41
% Usp[5]	—	—	—	—	—	0·9	—	—	—	—
% Ilm[6]	96·1	6·0	11·5	8·9	10·75(57)	—	12·4	11·4(21)	0·7(7)	1·25

Numbers in parentheses indicate one standard deviation of replicate analyses in terms of smallest units cited.
[1]Temperature (°C)/fO_2 (given relative to NNO) conditions of the charge. Italicized numbers are for a pressure of 50 MPa, all others for 150 MPa.
[2]n.d., not determined.
[3]Number of analyses.
[4]FeO and Fe_2O_3 calculated from formula constraints.
[5]Usp: mole fraction of ulvöspinel in the spinel oxide.
[6]Ilm: mole fraction of ilmenite in the rhombohedral oxide.

Table 6: Compositions of experimental accessory phases (wt %)

Run:	002-33	002-43	002-33	575-47	49-44	49-33	002-17	49-16	49-24	49-44	002-18	002-20
T/ΔNNO:[1]	693/−1·8	729/−3·2	693/−1·8	661/−1·7	661/−1·7	678/−1·7	752/4·3	775/3·6	679/3·9	661/−1·7	752/4·2	752/4·0
	fay	fay	bt	bt	bt	montd	chevk	chevk	chevk	chevk	tit	tit
n:[2]	2	1	1	1	3	1	1	1	1	2	2	1
SiO_2	32·29(102)	30·95	36·83	38·34	35·23(63)	43·29	18·88	16·80	17·34	16·32(21)	32·35(85)	33·76
TiO_2	0·08(11)	0·04	3·83	1·59	2·96(6)	1·07	17·06	17·54	13·77	17·21(4)	20·89(13)	20·69
Al_2O_3	0·62(18)	0·57	8·14	6·91	6·41(25)	1·45	0·48	0·07	0·24	0·04(3)	2·35(4)	3·03
FeO[3]	61·45(198)	64·16	34·42	31·83	39·19(94)	31·72	12·24	13·05	13·43	13·48(41)	8·15(3)	7·90
MgO	0·43(2)	0·77	2·20	0·48	0·63(8)	0·00	0·24	0·00	0·05	0·05(7)	0·37(0)	0·41
MnO	4·29(44)	2·78	0·91	0·40	0·31(4)	0·54	0·00	0·00	0·25	0·01(1)	0·08(6)	0·00
CaO	0·13(4)	0·08	0·00	0·00	0·00	0·05	5·28	2·38	1·71	0·97(1)	20·65(48)	20·85
Na_2O	0·44(34)	0·21	0·42	1·02	0·59(19)	0·32	0·07	0·00	0·26	0·01(1)	0·78(37)	0·48
K_2O	0·51(18)	0·22	8·15	7·49	8·33(25)	8·29	0·13	0·10	0·24	0·04(2)	0·48(4)	0·58
F	—	—	3·37	1·88	2·19(31)	7·72	0·94	1·20	0·88	1·20(8)	1·53(13)	2·04
Cl	—	—	0·25	0·18	0·07(7)	0·07	0·00	0·02	0·00	0·01(1)	0·00	0·00
Total	100·24	99·70	97·70	90·18	95·91	94·45	54·37	49·94	47·29	48·13	86·11	87·71
XFe[4]	0·92	0·94	0·88	0·96	0·96	0·98	0·97	1·00	0·98	0·99	0·92	0·91

Numbers in parentheses indicate one standard deviation of replicate analyses in terms of smallest units cited. fay, fayalite; bt, biotite; montd, montdorite; chevk, chevkinite; tit, titanite.
[1]Temperature (°C)/fO_2 (given relative to NNO) conditions of the charge. Italicized numbers are for a pressure of 50 MPa, all others for 150 MPa.
[2]Number of analyses.
[3]Total Fe as FeO.
[4]$X\text{Fe} = \text{Fe}/(\text{Fe} + \text{Mn} + \text{Mg})$, in moles.

Table 7: Compositions of experimental glasses (wt %)

Run:	002-3	002-6	002-7	002-8	002-9	002-10	002-11	002-15	002-16	002-17	002-18	002-19	002-20	002-21
T/ΔNNO:[1]	788/−1·4	738/−1·1	738/−1·1	699/−1·1	699/−1·2	*794/−1·5*	*794/−1·7*	794/4·1	794/3·9	752/4·3	752/4·2	752/4·1	752/4·0	752/3·9
n:[2]	7	7	10	6	6	6	6	5	5	5	5	6	2	2
SiO_2	76·31(70)	76·32(41)	76·88(85)	76·64(19)	76·92(39)	76·53(24)	77·09(38)	76·41(40)	77·55(32)	76·63(28)	76·81(9)	77·20(38)	76·76(30)	76·61(2)
Al_2O_3	12·09(55)	12·19(11)	11·96(17)	12·19(12)	11·98(15)	11·88(11)	11·92(12)	11·89(20)	11·48(20)	12·03(12)	11·83(11)	11·49(13)	11·54(20)	11·63(1)
FeO_{tot}[3]	1·41(16)	1·38(13)	1·40(14)	1·14(17)	1·23(11)	1·45(18)	1·31(13)	1·44(13)	1·32(13)	1·41(28)	1·31(10)	1·36(20)	1·49(14)	1·72(0)
MgO	0·03(2)	0·00(1)	0·01(1)	0·01(1)	0·03(2)	0·04(2)	0·02(2)	0·05(2)	0·06(1)	0·05(4)	0·04(2)	0·02(3)	0·04(2)	0·02(3)
MnO	0·07(8)	0·00	0·00	0·03(4)	0·06(7)	0·00	0·00	0·00	0·00	0·00	0·00	0·00	0·00	0·00
CaO	0·24(4)	0·29(4)	0·22(4)	0·23(3)	0·23(13)	0·31(11)	0·23(4)	0·37(5)	0·29(4)	0·38(3)	0·31(8)	0·28(3)	0·28(7)	0·21(6)
Na_2O	4·57(24)	4·74(11)	4·48(35)	4·55(17)	4·47(14	4·61(11)	4·08(20)	4·53(23)	3·89(10)	4·47(13)	4·57(9)	4·45(11)	4·36(14)	4·12(21)
K_2O	4·88(13	4·72(11)	4·54(24)	4·87(18)	4·45(15)	4·80(19)	4·93(14)	4·90(14)	4·93(8)	4·64(12)	4·78(9)	4·76(8)	4·84(9)	4·83(5)
TiO_2	0·12(3)	0·09(4)	0·08(5)	0·03(4)	0·03(3)	0·13(6)	0·09(3)	0·09(5)	0·11(7)	0·09(3)	0·07(4)	0·09(6)	0·04(4)	0·11(5)
F	0·28(8)	0·26(6)	0·43(5)	0·30(1)	0·60(11)	0·27(9)	0·32(8)	0·31(4)	0·37(7)	0·31(9)	0·29(5)	0·33(11)	0·65(6)	0·75(21)
Cl	0·35	n.d.[4]	n.d.	n.d.	0·21	n.d.	0·15	0·16	n.d.	n.d.	n.d.	n.d.	n.d.	0·26
H_2O[5]	2·8	4·6	4·2	4·9	4·2	3·7	2·8	3·5	2·1	4·7	4·2	3·9	3·0	2·6
Total	95·71	94·14	94·56	90·56	91·71	94·58	95·64	94·68	96·52	93·15	93·94	94·28	94·05	92·35
ZrO_2	n.d.	n.d.	n.d.	n.d.	n.d.	n.d.	n.d.	n.d.	n.d.	n.d.	n.d.	n.d.	n.d.	n.d.
NK/A[6]	1·06	1·06	1·03	1·05	1·02	1·08	1·01	1·07	1·02	1·03	1·07	1·08	1·07	1·03

Run:	002-22	002-23	002-24	002-25	002-28	002-29	002-30	002-33	002-34	002-35	002-38	002-42	002-43	002-44
T/ΔNNO:	788/−1·8	696/4·2	696/4·1	696/4·0	*790/−1·8*	*790/−1·9*	*790/−2·1*	693/−1·8	*756/−1·4*	*756/−1·5*	784/2·4	758/−3·1	729/−3·2	773/−3·1
n:	6	6	6	3	6	5	5	2	6	3	6	5	5	5
SiO_2	77·19(21)	77·09(17)	77·26(20)	76·05(23)	78·18(27)	77·76(37)	75·97(41)	73·37(28)	77·49(22)	75·20(11)	74·94(23)	73·75(30)	73·42(42)	74·21(38)
Al_2O_3	11·57(15)	12·33(9)	12·06(21)	12·30(18)	11·42(12)	11·11(11)	11·91(34)	10·77(28)	11·59(9)	11·02(4)	11·58(12)	11·28(9)	11·41(46)	11·77(19)
FeO_{tot}	1·44(16)	0·99(9)	1·09(22)	1·51(18)	0·79(12)	1·28(13)	1·33(22)	3·71(3)	1·16(12)	2·68(30)	1·84(20)	3·10(18)	3·28(21)	2·68(12)
MgO	0·03(2)	0·03(2)	0·02(2)	0·01(1)	0·05(3)	0·02(2)	0·03(2)	0·01(1)	0·02(2)	0·02(2)	0·02(3)	0·03(2)	0·02(2)	0·03(1)
MnO	n.d.	n.d.	n.d.	n.d.	n.d.	n.d.	n.d.	0·02(2)	0·06(7)	0·10(1)	0·05(4)	0·12(11)	0·08(8)	0·10(8)
CaO	0·26(6)	0·30(6)	0·26(6)	0·04(4)	0·22(3)	0·25(3)	0·28(4)	0·08(2)	0·17(7)	0·22(2)	0·18(4)	0·27(2)	0·11(2)	0·32(6)
Na_2O	4·10(10)	4·07(24)	4·24(20	4·05(41)	3·91(18)	3·91(17)	4·26(20)	5·42(24)	4·00(6)	4·27(16)	4·88(30)	4·64(14)	4·90(23)	4·52(13)
K_2O	4·83(10)	4·70(5)	4·41(11)	4·80(27)	4·70(12)	4·83(19)	5·07(19)	4·48(3)	4·91(13)	5·17(17)	5·03(15)	5·07(9)	4·88(16)	4·94(12)
TiO_2	0·14(3)	0·05(5)	0·02(3)	0·07(4)	0·11(6)	0·13(9)	0·19(3)	0·14(9)	0·10(6)	0·14(5)	0·12(11)	0·18(6)	0·18(5)	0·17(6)
F	0·45(5)	0·34(3)	0·45(7)	0·88(1)	0·42(5)	0·47(9)	0·65(13)	1·36(34)	0·34(10)	0·71(23)	0·96(7)	0·87(9)	1·06(12)	0·70(16)
Cl	0·29	0·10(5)	0·18(3)	0·28(7)	0·21(4)	0·24(5)	0·30(4)	0·58(2)	0·15(2)	0·46(2)	0·34(12)	0·68(8)	0·66(7)	0·57(5)
ZrO_2	n.d.	n.d.	n.d.	n.d.	n.d.	n.d.	n.d.	n.d.	n.d.	n.d.	n.d.	n.d.	n.d.	n.d.
H_2O	2·5	4·9	4·3	3·6	2·2	3·4	2·5	2·4	2·6	3·1	1·0	0·9	1·1	1·0
Total	96·03	91·96	91·97	89·97	97·30	95·85	96·93	88·57	96·43	95·81	95·60	94·75	92·89	96·21
NK/A	1·03	0·95	0·97	0·96	1·01	1·05	1·05	1·28	1·02	1·15	1·16	1·16	1·17	1·09

JOURNAL OF PETROLOGY VOLUME 44 NUMBER 10 OCTOBER 2003

Run:	575-16	575-21	575-22	575-23	575-24	575-25	575-26	575-27	575-28	575-29	575-33	575-34	575-35	575-36
T/ΔNNO:	805/3·1	757/3·0	788/−1·9	791/−2·1	791/−2·3	703/3·4	703/3·3	703/3·2	703/3·0	703/2·9	676/−1·6	676/−1·8	676/−2·0	678/4·0
n:	6	6	6	4	4	6	6	9	4	2	3	4	3	5
SiO_2	73·80(36)	73·96(29)	74·15(31)	69·61(30)	66·13(14)	75·19(64)	74·59(22)	73·78(24)	72·45(75)	71·74(20)	72·82(89)	71·73(52)	69·37(39)	74·82(25)
Al_2O_3	10·56(10)	10·67(34)	10·44(19)	9·10(9)	7·36(28)	10·70(15)	10·82(7)	10·58(18)	10·31(22)	9·77(21)	10·05(57)	10·25(14)	9·92(6)	10·62(11)
FeO_{tot}	4·10(33)	3·83(18)	4·04(14)	7·47(27)	10·21(35)	3·30(31)	3·29(16)	3·50(22)	4·36(9)	4·86(4)	4·47(16)	4·66(31)	5·11(18)	3·52(8)
MgO	0·01(2)	0·02(2)	0·01(2)	0·07(3)	0·07(3)	0·01(2)	0·01(1)	0·02(3)	0·04(1)	0·02(2)	0·00	0·01(1)	0·00	0·02(3)
MnO	0·06(6)	0·06(6)	n.d.	0·43	0·44(13)	n.d.	n.d.	n.d.	n.d.	n.d.	0·04(1)	0·03(3)	0·10(6)	0·04(5)
CaO	0·09(5)	0·05(4)	0·08(4)	0·19(3)	0·42(5)	0·05(3)	0·07(4)	0·04(3)	0·03(3)	0·00	0·05(4)	0·06(5)	0·09(4)	0·02(3)
Na_2O	5·64(18)	5·44(17)	5·65(14)	6·66(12)	8·42(31)	5·00(22)	5·31(7)	5·90(23)	6·08(68)	6·03(57)	5·75(25)	6·32(31)	7·20(15)	5·09(20)
K_2O	4·57(8)	4·68(9)	4·44(11)	4·68(10)	4·60(23)	4·54(22)	4·45(14)	4·55(11)	4·56(11)	4·56(30)	4·17(32)	4·18(18)	3·56(2)	4·48(8)
TiO_2	0·11(8)	0·12(6)	0·15(4)	0·37(5)	0·69(7)	0·14(6)	0·15(4)	0·20(5)	0·23(1)	0·32(4)	0·23(3)	0·22(6)	0·34(2)	0·14(3)
F	1·05(9)	1·16(9)	1·04(4)	1·85(13)	2·07(19)	0·88(8)	0·96(10)	1·02(9)	1·53(5)	2·05(4)	1·82(12)	1·90(9)	3·48(14)	0·94(6)
Cl	n.d.	0·38	n.d.	0·98	1·50(15)	0·19(5)	0·36(5)	0·42(3)	0·42(5)	0·65(21)	0·58(1)	0·55(8)	0·73(2)	0·17(1)
ZrO_2	n.d.	n.d.	n.d.	0·42	1·53(37)	0·28	0·66	0·61	0·45	0·83				
H_2O	2·4	2·7	2·5	0·8	0·0	5·8	4·8	4·0	3·2	2·5	4·0	3·0	1·9	5·8
Total	96·23	95·86	96·24	96·70	95·34	91·42	91·57	92·60	89·70	90·52	91·42	91·61	91·72	91·59
NK/A	1·35	1·31	1·35	1·76	2·56	1·23	1·25	1·38	1·45	1·52	1·39	1·46	1·58	1·24

Run:	575-37	575-38	575-42	575-43	575-44	575-45	575-46	575-47	575-48	575-50	575-51	575-53	575-56	575-57
T/ΔNNO:	678/3·9	678/3·8	786/3·7	786/3·5	*737/−1·4*	*737/−1·6*	*737/−1·9*	661/−1·7	702/−1·9	702/−2·6	784/2·4	*686/−2·1*	758/−3·1	729/−3·2
n:	5	6	5	5	5	4	3	5	5	1	7	5	5	4
SiO_2	74·55(31)	72·55(31)	72·12(26)	72·39(38)	73·65(42)	72·97(57)	69·96(34)	75·15(59)	71·07(34)	66·05	70·20(6)	70·81(37)	69·76(17)	67·46(29)
Al_2O_3	10·56(7)	10·84(10)	9·67(9)	9·89(7)	10·48(11)	10·14(23)	9·40(16)	10·59(15)	9·96(8)	10·18	9·46(8)	9·57(16)	9·61(13)	9·20(34)
FeO_{tot}	3·49(38)	3·35(18)	5·36(10)	5·10(14)	3·94(31)	3·82(32)	6·09(23)	3·01(8)	4·95(22)	5·20	5·77(25)	5·39(20)	5·44(23)	7·19(18)
MgO	0·01(1)	0·01(1)	0·03(2)	0·03(2)	0·01(1)	0·03(2)	0·03(5)	0·01(1)	0·02(3)	0·00	0·03(3)	0·03(3)	0·02(2)	0·04(1)
MnO	0·14(7)	0·06(7)	0·25(6)	0·07(6)	0·14(4)	0·11(8)	0·11(2)	0·03(5)	0·11(13)	0·20	0·19(9)	0·12(8)	0·17(10)	0·24(14)
CaO	0·01(1)	0·01(2)	0·06(5)	0·05(3)	0·10(5)	0·09(5)	0·09(3)	0·04(2)	0·05(3)	0·05	0·04(2)	0·02(2)	0·13(4)	0·07(2)
Na_2O	5·32(17)	6·15(30)	5·63(11)	5·38(10)	5·3923)	5·92(13)	6·63(26)	6·00(46)	6·85(33)	8·59	6·07(13)	6·69(22)	6·87(20)	7·31(37)
K_2O	4·50(11)	4·59(13)	4·86(9)	4·93(8)	4·70(16)	4·87(16)	4·66(21)	4·21(15)	4·30(12)	4·23	5·10(13)	4·23(10)	4·75(11)	4·22(28)
TiO_2	0·13(3)	0·207)	0·26(5)	0·22(4)	0·16(4)	0·24(3)	0·27(5)	0·04(4)	0·21(8)	0·36	0·34(3)	0·32(6)	0·29(10)	0·37(5)
F	0·97(11)	1·84(14)	1·49(9)	1·39(16)	0·96(8)	1·27(5)	1·90(9)	0·70(17)	1·68(12)	4·26	2·20(8)	2·05(23)	2·16(7)	2·88(53)
Cl	0·28(2)	0·37(5)	0·22(4)	0·47(3)	0·47(4)	0·50(5)	0·81(5)	0·22(8)	0·77(9)	0·89	0·55(4)	0·75(7)	0·80(4)	1·01(11)
ZrO_2	n.d.	n.d.	n.d.	n.d.	n.d.	0·57	n.d.	n.d.	n.d.	n.d.	n.d.	n.d.	n.d.	n.d.
H_2O	5·1	4·2	1·9	3·3	3·3	3·8	2·6	5·8	2·8	0·3	0·9	3·3	0·8	1·3
Total	92·04	92·23	97·49	97·33	95·57	94·98	96·46	90·63	93·74	100·00	96·79	92·14	96·20	95·02
NK/A	1·29	1·39	1·50	1·44	1·33	1·48	1·70	1·36	1·60	1·84	1·64	1·63	1·71	1·80

Table 7: continued

Run:	575-58	49-7	49-9	49-16	49-17	49-18	49-19	49-20	49-21	49-22	49-23	49-24	49-25	49-26
T/ΔNNO:	773/−3·1	744/−1·1	703/−1·2	775/3·6	725/4·1	725/3·9	725/3·9	725/3·7	725/3·7	796/−1·8	796/−2·0	679/3·9	679/3·8	679/3·7
n:	5	7	6	7	7	6	7	8	7	6	6	6	6	7
SiO_2	70·86(63)	73·62(31)	74·09(28)	73·55(30)	74·11(34)	74·18(45)	73·68(32)	72·82(32)	72·05(47)	74·19(38)	71·07(19)	74·77(42)	73·42(29)	72·14(26)
Al_2O_3	10·60(49)	10·79(8)	10·54(15)	10·32(15)	10·65(12)	10·62(10)	10·65(15)	10·29(33)	9·97(19)	10·64(11)	10·11(20)	10·68(17)	10·71(19)	11·17(13)
FeO_{tot}	4·06(21)	3·80(22)	3·74(11)	4·30(22)	3·69(28)	3·71(19)	3·94(27)	4·51(22)	5·15(34)	3·40(14)	4·58(16)	3·39(14)	3·81(15)	3·42(22)
MgO	0·03(3)	0·02(1)	0·01(1)	0·01(2)	0·03(3)	0·01(2)	0·01(2)	0·00(1)	0·03(2)	0·01(2)	0·01(1)	0·03(2)	0·03(2)	0·01(1)
MnO	0·15(13)	0·00	0·04(2)	0·10(9)	0·11(8)	0·04(3)	0·04(4)	0·13(6)	0·06(7)	n.d.	0·16	n.d.	n.d.	0·15
CaO	0·12(3)	0·07(4)	0·06(4)	0·06(3)	0·04(4)	0·06(4)	0·06(5)	0·04(4)	0·03(2)	0·09(3)	0·10(5)	0·04(2)	0·01(2)	0·01(2)
Na_2O	6·80(21)	5·76(13)	5·74(16)	5·70(18)	5·74(13)	5·75(35)	5·92(22)	5·87(24)	6·08(32)	5·70(17)	6·74(11)	5·34(33)	5·75(25)	6·10(13)
K_2O	4·93(20)	4·57(7)	4·54(3)	4·65(11)	4·37(6)	4·47(8)	4·56(14)	4·80(13)	4·80(13)	4·66(13)	5·00(9)	4·32(8)	4·48(14)	4·59(12)
TiO_2	0·27(4)	0·18(7)	0·12(5)	0·18(6)	0·12(4)	0·11(10)	0·13(6)	0·17(5)	0·22(7)	0·21(4)	0·30(7)	0·14(8)	0·14(4)	0·18(4)
F	1·56(17)	1·20(11)	1·12(13)	1·12(6)	1·14(10)	1·04(13)	1·02(12)	1·37(16)	1·60(12)	1·10(9)	2·09(20)	1·09(11)	1·31(13)	1·93(14)
Cl	0·61(14)	n.d.	n.d.	n.d.	n.d.	n.d.	n.d.	0·46	n.d.	n.d.	0·78	0·20(4)	0·34(2)	0·45(5)
ZrO_2	n.d.	n.d.	n.d.	n.d.	n.d.	n.d.	n.d.	n.d.	n.d.	n.d.	0·68	n.d.	n.d.	0·40
H_2O	0·7	3·5	5·2	2·8	5·7	4·9	4·1	4·2	3·7	3·0	2·5	5·7	5·0	4·5
Total	97·78	95·28	92·52	95·68	92·35	93·25	94·19	94·08	95·03	96·86	95·53	91·31	92·08	91·34
NK/A	1·56	1·34	1·36	1·40	1·33	1·35	1·38	1·44	1·53	1·35	1·63	1·26	1·34	1·34

Run:	49-27	49-32	49-33	49-35	49-36	49-37	49-38	49-39	49-40	49-42	49-43	49-44	49-45	49-46
T/ΔNNO:	679/3·6	678/−1·6	678/−1·7	700/3·1	700/3·0	700/2·9	700/2·7	786/3·3	786/2·8	*732/−1·6*	*732/−1·9*	661/−1·7	702/−2·0	702/−2·1
n:	4	2	5	5	5	5	1	6	5	6	5	5	3	4
SiO_2	70·67(22)	70·96(24)	69·87(40)	73·47(25)	72·18(28)	70·13(20)	68·31	72·50(37)	71·08(22)	73·02(24)	69·45(42)	74·22(45)	70·32(42)	69·06(20)
Al_2O_3	11·67(15)	10·50(11)	10·11(7)	10·32(13)	10·52(9)	10·86(11)	11·67	9·87(10)	9·53(16)	10·20(17)	9·54(21)	10·52(14)	9·91(17)	9·61(12)
FeO_{tot}	3·04(9)	4·98(9)	5·32(38)	4·01(26)	4·12(17)	3·84(12)	3·96	4·96(33)	5·44(25)	3·83(11)	5·47(43)	3·38(30)	5·35(14)	5·92(17)
MgO	0·01(1)	0·02(2)	0·03(2)	0·01(1)	0·01(1)	0·01(1)	0·00	0·03(2)	0·02(4)	0·02(3)	0·04(3)	0·01(2)	0·01(1)	0·03(2)
MnO	0·31	0·04(4)	0·10(5)	0·07(4)	0·04(5)	0·02(2)	0·18	0·04(4)	0·06(7)	0·03(4)	0·16(9)	0·11(7)	0·10(9)	0·16(9)
CaO	0·00(0)	0·02(0)	0·05(4)	0·05(2)	0·01(1)	0·02(2)	0·00	0·06(2)	0·05(4)	0·05(3)	0·08(3)	0·03(2)	0·08(2)	0·07(2)
Na_2O	6·36(26)	6·30(13)	6·97(24)	5·44(18)	5·80(9)	6·35(22)	6·76	5·20(11)	5·87(15)	5·94(9)	6·94(19)	6·13(32)	6·91(13)	7·28(30)
K_2O	4·65(10)	3·98(3)	3·88(18)	4·71(5)	4·76(17)	5·06(9)	5·28	4·95(18)	5·04(10)	4·74(16)	4·81(14)	4·26(11)	4·22(19)	4·25(12)
TiO_2	0·17(6)	0·31(2)	0·29(4)	0·14(4)	0·20(6)	0·27(5)	0·21	0·24(5)	0·27(2)	0·27(4)	0·37(7)	0·09(6)	0·25(9)	0·35(2)
F	2·85(13)	2·09(6)	2·58(29)	1·30(8)	1·87(6)	2·85(12)	3·08	1·65(11)	2·10(11)	1·29(14)	2·31(16)	0·99(11)	1·90(33)	2·25(7)
Cl	0·59(4)	0·69(0)	0·79(6)	0·40(1)	0·48(9)	0·58(6)	0·55	0·49(3)	0·52(5)	0·58(9)	0·82(8)	0·25(5)	0·93(3)	1·01(9)
ZrO_2	0·80	n.d.	n.d.	n.d.	n.d.	n.d.	n.d.	n.d.	n.d.	0·25	n.d.	n.d.	n.d.	n.d.
H_2O	3·9	4·6	4·0	4·9	4·0	3·3	3·0	2·8	2·4	3·4	3·0	5·7	3·7	3·0
Total	91·65	91·20	92·94	93·79	94·90	93·77	94·00	96·36	96·80	95·46	95·92	89·92	90·66	94·29
NK/A	1·33	1·40	1·55	1·36	1·40	1·46	1·44	1·41	1·59	1·46	1·74	1·40	1·61	1·73

Run:	49-48	49-52	49-53	49-54	49-55	49-58	49-59	49-60
T/ΔNNO:	784/2·2	731/n.d.	731/n.d.	731/0·1	679/−1·9	758/−3·1	729/−3·2	773/−3·1
n:	4	5	4	4	6	4	4	5
SiO_2	67·28(28)	73·72(18)	72·55(13)	63·97(97)	69·71(51)	68·46(63)	63·74(45)	69·43(12)
Al_2O_3	9·35(9)	10·51(16)	10·22(14)	8·57(42)	9·26(7)	9·52(16)	8·44(27)	10·16(18)
FeO_{tot}	6·43(29)	3·51(14)	4·39(7)	7·37(58)	6·42(30)	6·10(28)	8·83(26)	4·60(23)
MgO	0·01(1)	0·01(2)	0·00(0)	0·02(2)	0·03(2)	0·03(3)	0·01(2)	0·01(2)
MnO	0·18(12)	0·10(10)	0·09(8)	0·20(11)	0·13(7)	0·14(11)	0·26(7)	0·09(6)
CaO	0·04(3)	0·15(5)	0·05(2)	0·05(3)	0·05(3)	0·10(4)	0·09(2)	0·12(3)
Na_2O	6·75(9)	6·07(23)	5·93(20)	8·94(87)	6·72(21)	6·92(86)	8·13(25)	7·26(11)
K_2O	5·13(18)	4·45(9)	4·61(9)	4·89(21)	4·25(17)	4·67(12)	4·57(23)	4·98(11)
TiO_2	0·53(3)	0·05(4)	0·21(8)	0·70(2)	0·29(4)	0·24(13)	0·56(6)	0·33(5)
F	3·63(6)	0·96(9)	1·35(9)	4·30(45)	2·14(26)	2·89(23)	4·28(55)	2·25(10)
Cl	0·65(3)	0·43(6)	0·50(5)	0·96(4)	0·97(4)	0·93(8)	1·10(18)	0·78(3)
ZrO_2	n.d.	n.d.	n.d.	n.d.	n.d.	n.d.	n.d.	n.d.
H_2O	1·5	4·4	3·3	1·6	2·5	1·1	1·4	1·0
Total	96·67	95·54	94·81	95·40	94·90	96·27	96·41	96·06
NK/A	1·78	1·41	1·44	2·33	1·69	1·73	2·17	1·70

Only glasses of crystal-bearing charges are listed. All analyses normalized to 100% anhydrous. Original totals after alkali correction reported. Numbers in parentheses indicate one standard deviation of replicate analyses in terms of smallest units cited.
[1]Temperature (°C)/fO_2 (given relative to NNO) conditions of the charge. Italicized numbers are for a pressure of 50 MPa, all others for 150 MPa.
[2]Number of analyses.
[3]Total Fe as FeO.
[4]n.d., not determined.
[5]H_2O determined using the difference to 100% method or mass balance constraints (see Scaillet & Macdonald, 2001).
[6]NK/A: $(Na_2O + K_2O)/Al_2O_3$, in moles.

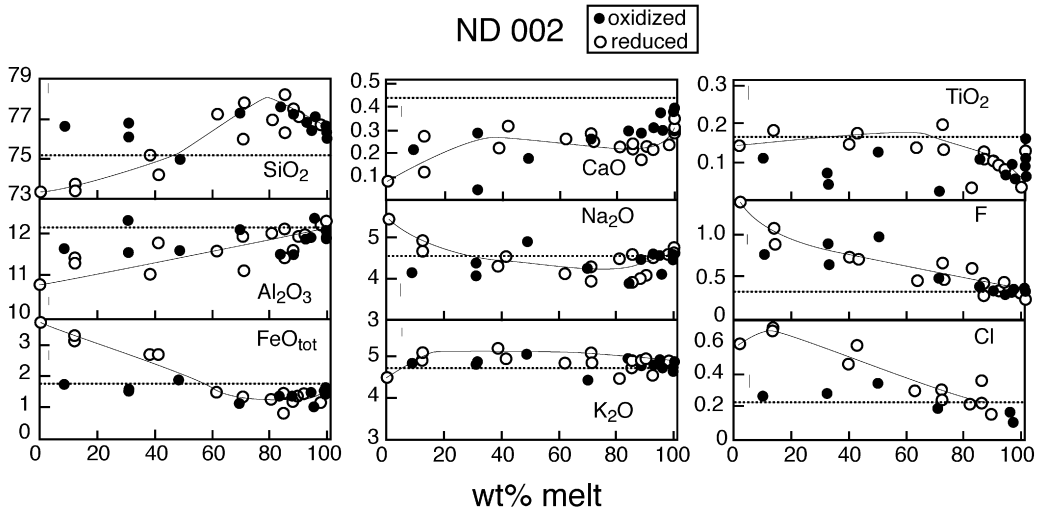

Fig. 7. Major element abundances plotted against degree of crystallization in ND002, for both reduced and oxidized conditions. The continuous line represents the trend obtained under reduced conditions. The dashed line represents the bulk composition. The vertical bars represent the average standard deviation of electron microprobe analyses (see Table 7).

bulk compositions. A slight decrease in FeO* content is apparent under reduced conditions but it never exceeds 6% of the original FeO* content. In the following, liquids produced by the crystallization of ND002 are considered first, then trends obtained with both BL575 and SMN49 compositions are shown together, as they display virtually identical geochemical behaviour, in keeping with their similar bulk compositions.

ND002

The variations of all relevant oxides with crystallization are shown in Fig. 7. When, at low fO_2, the degree of crystallization remains moderate (<40%), residual liquids are marked by a slight increase in SiO_2 and decreases in FeO, CaO, TiO_2 and, to a lesser extent, Al_2O_3. K_2O remains roughly constant, although it can increase slightly (to over 5 wt %) in some charges. Na_2O shows no systematic variation and the NK/A ratios of residual liquids scatter around that of the starting composition. These trends are observed irrespective of fO_2 conditions and mainly reflect the crystallization of clinopyroxene (FeO, CaO), oxide (FeO, TiO_2) and alkali feldspar (Al_2O_3), and the dominantly incompatible behaviour of F and Cl.

At low fO_2 in heavily crystallized charges, the residual melt compositions differ significantly from the starting composition, as a result of clinopyroxene being unstable and breaking down to fayalite + magnetite + fluorite assemblages. In all such charges, the liquid SiO_2 and Al_2O_3 contents are either equal to, or lower than, those in the starting composition but the FeO* content increases up to nearly twice the original value. K_2O remains remarkably constant whereas the Na_2O contents, and by implication the NK/A ratios, of the liquid also increase. The abundances of F and Cl reach 1 wt % and 0·68 wt %, respectively. The residual melt composition in the near-solidus charge 33 closely approaches that of bulk-rock compositions SMN49 or BL575 and we can say that after 75% crystallization, the melt has evolved to a composition close to, but on the comenditic side of, the comendite–pantellerite boundary in Fig. 2.

At high fO_2, the residual melts do not achieve the same levels of peralkalinity as at lower fO_2, even when >90 wt % crystallized. An exception is charge ND38, which is a fluid-absent run in which fO_2 might be lower than our estimate (Scaillet & Macdonald, 2001). Charges crystallized at $T > 750°C$ show only a slight increase in NK/A, to ~1·09 (Table 7). At lower temperatures, the residual melt compositions are less peralkaline, some even being peraluminous (charges 23–25; Table 7). The maxima in Cl content do not exceed 0·3 wt %.

The reason for the contrasting behaviour between low and high fO_2 conditions can readily be seen using an FeO^*–Al_2O_3–(Na_2O + K_2O) projection (Fig. 8). At low fO_2, feldspar, clinopyroxene and melt (+ oxides, biotite and fayalite) are essentially collinear, all three lying close to, but on the peralkaline side of, the peraluminous–peralkaline divide. Clinopyroxene and feldspar exert opposing effects on melt peralkalinity, which remains broadly constant when these two phases are stable. In contrast, when conditions preclude clinopyroxene crystallization (high fF_2,

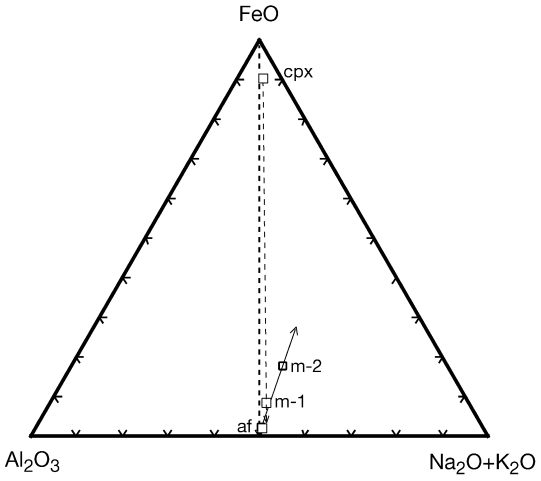

Fig. 8. Positions of selected ND002 melt compositions connected to coexisting minerals by tie-lines in the FeO^*–Al_2O_3–($Na_2O + K_2O$) ternary diagram, illustrating the opposing effects of feldspar and clinopyroxene on melt composition. Two topological arrangements are shown: one in which clinopyroxene (cpx) coexists with feldspar (af), counteracting its effect on melt (m-1) peralkalinity; the other represents a case without clinopyroxene, whereby the melt (m-2) peralkalinity increases owing to the crystallization of a less peralkaline feldspar. The continuous tie-line represents the effect of feldspar on melt composition, the dashed tie-line that of clinopyroxene. Melt compositions are from charges 002-7 (m-1) and 002-33 (m-2). Clinopyroxene composition is from charge 002-4. For clarity, other accessory phases such as biotite, olivine and ilmenite have not been plotted.

low melt H_2O content or low temperature at low fO_2), melt peralkalinity increases in response to feldspar fractionation, as feldspar is less peralkaline than coexisting melt. This is because clinopyroxene breaks down into fayalite + magnetite, with a negligible role in melt peralkalinity. Although crystallization of sodic amphibole might dampen this increase in sodium, mass balance calculations show that this phase occurs in such small amounts in ND002-type rhyolites under the conditions explored (Table 1) that it has virtually no effect on melt composition. In addition, amphibole is not stable everywhere along the solidus in ND002 (Scaillet & Macdonald, 2001), and the most peralkaline melt produced from crystallization of ND002 does not coexist with amphibole.

At high fO_2, the clinopyroxene stability field widens considerably (Scaillet & Macdonald, 2001) and neither fayalite nor magnetite appears to be stable. As a result, the clinopyroxene control on melt composition is magnified. Clinopyroxene crystallizing at *c.* 780°C is strongly peraluminous, which explains the slight increase in melt peralkalinity as crystallization proceeds at this temperature. In contrast, at around 700°C, pyroxene compositions shift towards the peralkaline field, which drives the coexisting melt towards a more metaluminous composition. Because the modal amounts of pyroxene are always low (<2 wt %; Table 1), it may be difficult to envisage a major petrogenetic role for this phase, especially when compared with that of feldspar. Whereas this might be true for strongly peralkaline melts, it is not for those that are only slightly Al deficient, such as ND002. For example, congruent dissolution of only 3 wt % of a clinopyroxene having 3 wt % Na_2O in a melt of ND002 composition with an NK/A of 1·046 would yield a melt having an NK/A of 1·059. As small as it might appear, this compositional shift is important because it produces a melt that is now more peralkaline than any feldspar crystallizing from ND002 (NK/A <1·05, Fig. 5). Without a clinopyroxene contribution, an ND002 type rhyolite crystallizing 60 wt % feldspar (NK/A of 1·045) and 30 wt % quartz would produce a residual liquid having an NK/A of 1·07, a value that is only marginally higher than that of the parent magma. In contrast, if clinopyroxene breaks down, the residual liquid produced after 60 wt % of feldspar fractionation (NK/A 1·045) would have an NK/A of 1·29, i.e. that of a typical comendite. Although the above values depend on the chosen value of feldspar peralkalinity, they serve to illustrate our main point: the feldspar control on liquid peralkalinity can be greatly exacerbated by a clinopyroxene contribution. Clinopyroxene stability appears thus to be the fundamental factor in determining melt peralkalinity in ND002-type rhyolites, by affecting the alkali/alumina balance between feldspar and residual melt. The critical stage is when feldspar and melt peralkalinities cross, after which feldspar fractionation merely increases the peralkalinity (e.g. Bailey & Macdonald, 1969). By analogy with the roles attributed to plagioclase and alkali feldspar in promoting Al deficiency in silicic melts, we call this the clinopyroxene effect.

BL575 and SMN49

Compared with ND002, there is in BL575 and SMN49 a much stronger change of melt composition with crystallization, with variations of several weight percent in most oxides (Fig. 9). The trends can be conveniently discussed in terms of the presence or absence of amphibole and/or aegirine. Under conditions where either phase is unstable, i.e. mostly at $T > 750$°C, the residual liquids trend toward SiO_2 and Al_2O_3 depletion and FeO^* and Na_2O enrichment (Fig. 9). As a result, melt peralkalinity continuously increases during fractionation, first resulting in melts closely similar to the natural Eburru pantellerites (Fig. 2) and then reaching

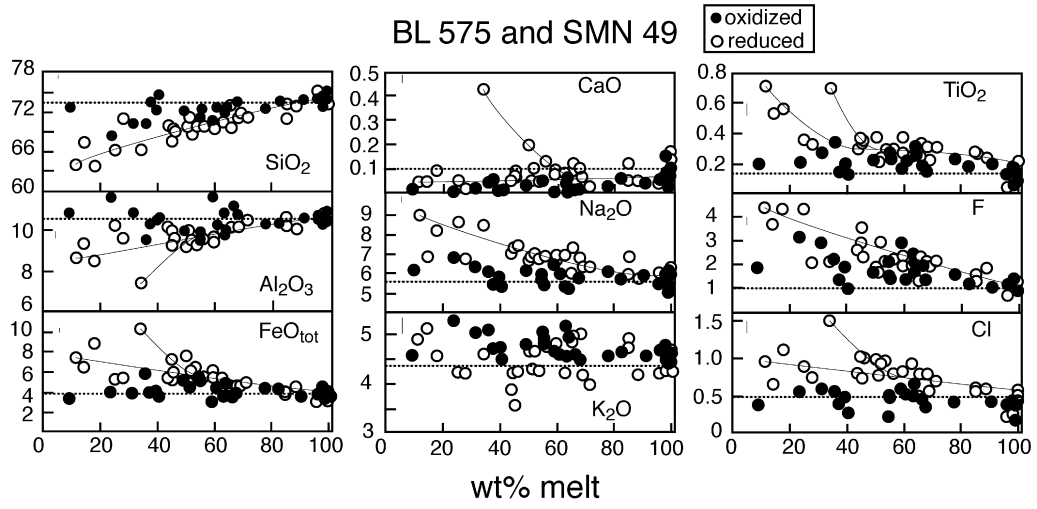

Fig. 9. Major element abundances plotted against degree of crystallization for BL575 and SMN49, for both reduced and oxidized conditions. The two continuous lines represent the trends obtained under reduced conditions with or without the crystallization of sodic amphibole, the former case being characterized by higher values of FeO_{tot}, TiO_2, CaO being reached at lower melt fractions relative to when amphibole precipitates. The dashed line represents the bulk composition of SMN49, which is similar to that of BL575 except for a higher CaO content (0·1 wt % in BL575). The vertical bars represent the average standard deviation of electron microprobe analyses (see Table 7).

values around 2·5, which are similar to the most extreme natural pantelleritic liquids (Macdonald & Bailey, 1973). Comendite crystallization yields the first pantelleritic derivatives after only 25% crystallization and the most extreme compositions after 66% crystallization (Table 1). This is achieved in SMN49 by a major decrease in SiO_2 content from ~75 wt % to <65 wt %, accompanied by an increase in melt FeO* content to >10 wt % and Al_2O_3 decrease to 7 wt %. It should be stressed that the major element compositions of these residual melts are indistinguishable from those of natural pantelleritic obsidians compiled by Macdonald & Bailey (1973).

Crystallization of strongly sodic phases either slows down (arfvedsonite) or arrests (aegirine) the trend towards peralkalinity, as illustrated in the FeO*–Al_2O_3–(Na_2O + K_2O) projection (Fig. 10). Aegirine crystallization in comendite magma constrains the residual liquids to NK/A <1·5. The effect of arfvedsonite crystallization on residual liquids is less marked but still, under our experimental conditions, most arfvedsonite-bearing liquids appear to have NK/A <1·6. In the case of aegirine, that is, under high fO_2, two additional effects are notable. Aegirine precipitation inhibits the iron enrichment trend and increases significantly the Al_2O_3 content of the liquid, the latter effect being responsible for the lack of peralkalinity increase in aegirine-bearing charges (Fig. 10). Finally, with respect to K_2O, the crystallization of the sodic phases seems to operate in opposite senses: aegirine fractionation increases slightly the liquid K_2O content, whereas arfvedsonite may decrease it.

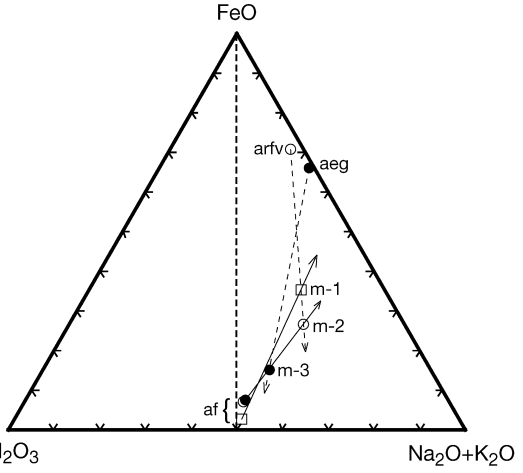

Fig. 10. Positions of selected BL575 and SMN49 melt compositions connected to coexisting minerals by tie-lines in the FeO*–Al_2O_3–(Na_2O + K_2O) ternary diagram, illustrating the opposing effects of feldspar, aegirine and alkali amphibole on melt composition. Three topological arrangements are shown: one (□) in which feldspar is the sole Na-bearing crystallizing phase, in which case the melt (m-1) peralkalinity increases continuously; a second case (○) in which the effect of feldspar on melt composition (m-2) is counteracted by the crystallization of an alkali amphibole (arfv); a third case (●), corresponding to high fO_2 conditions, in which the effect of feldspar on melt composition (m-3) is counteracted by the crystallization of aegirine (aeg). The continuous tie-lines represent the effect of feldspar on melt compositions, the dashed tie-lines that of amphibole and clinopyroxene. Phase compositions are from charges 575-24 (□), 49-54 (○) and 49-37 (●).

The TiO_2 and CaO contents tend to either decrease or remain constant in all charges with NK/A $<1{\cdot}5$. At higher values of the index, however, the abundances of both oxides increase with crystallization. The TiO_2 contents of the most fractionated liquids are close to 0·8 wt %. Most remarkable is the increase seen in CaO content. Despite extensive alkali feldspar crystallization, a four-fold increase in liquid CaO content, relative to the original bulk-rock value, is observed in the most pantelleritic liquids produced. This underlines the complete lack of CaO in the crystallizing feldspar, as shown above, presumably a result of the overall low temperatures of the experiments. Feldspar phenocrysts in peralkaline rhyolites, including those at Olkaria, typically have CaO abundances and CaO/(Na_2O + K_2O) ratios lower than the associated glasses or host rocks (Noble *et al*., 1971; Macdonald *et al*., 1987; Mahood & Stimac, 1990).

In all charge series, F and Cl contents gradually increase with progressive crystallization, to maxima slightly over 4 wt % for F and 1 wt % for Cl. A difference in behaviour related to fO_2 can be detected for Cl; as in ND002, Cl reaches higher concentrations at low fO_2. In both cases, this is possibly due to the higher content in Fe^{2+} of the melts that favours the existence of FeCl dissolved complexes. Zirconium was analysed in a few selected heavily crystallized charges in both BL575 and SMN49 (Table 7) and, as expected in peralkaline systems, the residual liquids show pronounced Zr enrichment, to 1·5 wt % ZrO_2 in the melt having the most extreme pantelleritic character of those analysed for Zr (charge 575-24, Table 6).

DISCUSSION

The phases controlling major element trends are quartz and feldspar and, in the least peralkaline compositions, clinopyroxene. Where only quartz and feldspar crystallize, the increase in peralkalinity of the residual melts seems limitless, as the feldspar is less peralkaline than the coexisting melt (Fig. 5). Our most extreme composition, with 10 wt % FeO* and 7·4 wt % Al_2O_3, is much more peralkaline than most pantellerites, being approached among bulk rocks only by a pantellerite from the Fantalé volcano, Ethiopia (Lacroix, 1930; Fig. 2). Mungall & Martin (1996) reported even more extreme compositions (Al_2O_3 5·0–5·5 wt %; FeO* 11·3–13·3 wt %), occurring as glass inclusions in fayalite phenocrysts and as interstitial glass in pantellerites of the Pico Alto volcano, Terceira, Azores. As there is no obvious reason for the increase in peralkalinity to stop, it can be anticipated that further crystallization of bulk-rock compositions such as BL575 or SMN49 may lead to pantelleritic derivatives with even more extreme compositions (i.e. FeO* >10 wt %) than those reported here. Only when either sodic amphibole or aegirine crystallizes is this increase in peralkalinity affected (Fig. 10). Experiments under oxidizing conditions show that the crystallization of aegirine in comendites restricts residual melts to NK/A $< \sim 1{\cdot}5$, whereas, at low fO_2, the crystallization of arfvedsonite at the level of several weight percent slows down the increase in peralkalinity. This suggests that any liquid line of descent in peralkaline silicic magmas will have its peralkalinity maximum controlled by the stability fields of sodic phases. This is in all respects similar to peraluminous silicic liquids crystallizing muscovite, whose precipitation buffers melt peraluminosity (Scaillet *et al*., 1995).

For weakly peralkaline magmas, our data highlight the important role played by clinopyroxene. While clinopyroxene is stable, there is little chance of producing derivative liquids significantly more peralkaline than the parental liquid. Therefore, the origin of the peralkaline tendency displayed by Ca-poor, silicic magmas must be in large part due to factors that control pyroxene stability. Our phase equilibrium study (Scaillet & Macdonald, 2001) and the present compositional data show that temperature, water activity, melt composition and fO_2 affect clinopyroxene stability and composition. The fugacities of F-bearing volatile species may be an additional factor (Bohlen & Essene, 1978). Most important are the redox conditions imposed during crystallization. Low fO_2 destabilizes clinopyroxene into a fayalite–ilmenite ± fluorite assemblage, whereas high fO_2 expands its stability field and inhibits olivine and ilmenite crystallization. These observations can be compared with those of Xirouchakis & Lindsley (1998) in the CaO–FeO–Fe_2O_3–TiO_2–SiO_2 synthetic system, where the maximum stability of hedenbergite with respect to fO_2 is given by

$$\text{hedenbergite} + \text{magnetite} \leftrightarrow \text{fayalite} + \text{ilmenite} + \text{quartz} \quad (1)$$

which qualitatively agrees with our observations (Scaillet & Macdonald, 2001). The maximum fO_2 of this reaction in the synthetic system is slightly below FMQ, whereas in our experiments Ca-bearing pyroxene persists well above this fO_2. This is because, first, Mg is present in ND002 and thus substitutes for Fe in the pyroxene, and, second, the activity of the ilmenite melt component is significantly below unity, both factors contributing to a significant displacement of reaction (1) towards higher fO_2. At low fO_2, hedenbergite (magnetite + quartz) breaks down into ilmenite and fayalite:

$$\text{hedenbergite} + \text{magnetite} + \text{quartz} \leftrightarrow \text{fayalite} + \text{ilmenite} \quad (2)$$

in agreement with our observations (Scaillet & Macdonald, 2001). In the synthetic system at 150 MPa, reaction (2) occurs at NNO − 1 at 700°C and at NNO − 1·4 at 800°C (Xirouchakis & Lindsley, 1998). This agrees closely with our results: in ND002 at 788°C and NNO − 1·37, no fayalite was detected, whereas at NNO − 1·4 fayalite is present (Table 1). Below 700°C, no hedenbergite was observed for fO_2 below NNO − 1·6, whereas both fayalite and ilmenite are present (charge 33, Table 1). The good agreement between our results and those of Xirouchakis & Lindsley (1998) stresses the point that ferromagnesian minerals crystallizing from peralkaline rhyolites under low fO_2 have compositions close to end-member. We suggest, therefore, that in Ca- and Mg-poor, reduced, peralkaline silicic magmas, the occurrence of clinopyroxene, and thus its role in melt peralkalinity, are partly controlled by reaction (2).

Calcium released by hedenbergite in reaction (2) is partly accommodated in fayalite but also, in ND002, in fluorite, as textural evidence of pyroxene breakdown products suggests (Scaillet & Macdonald, 2001). The latter observation, and thermodynamic calculations (Bohlen & Essene, 1978), show that the fugacities of F-bearing volatile species, such as fF_2, play a role in destabilizing the clinopyroxene, and thus in the development of peralkaline conditions. According to Bohlen & Essene (1978), the following reaction accounts for clinopyroxene stability relative to fF_2:

$$\text{hedenbergite} + F_2 \leftrightarrow \text{quartz} + \text{fluorite} + \text{fayalite} + O_2. \quad (3)$$

A bulk F content lower than that of ND002 may delay clinopyroxene breakdown to lower water activities relative to those observed in our experiments and thus inhibit the increase in melt peralkalinity over much of the crystallization interval of otherwise similar ND002-type rhyolites. Similarly, magmas poorer in F may not crystallize fluorite, which, in turn, may favour the appearance of other sodic–calcic phases, such as richterite, in greater abundances upon clinopyroxene breakdown: this may suppress the sodium enrichment of the melt consequent on pyroxene breakdown.

More generally, the new experiments constrain possible causes of peralkalinity in silicic magmas. Variations in fO_2 have already been invoked to explain diverging geochemical trends in peralkaline series (Mungall & Martin, 1995). Clearly, silicic magmas of identical bulk compositions but crystallizing under different redox conditions (and/or fF_2) may, or may not, give rise to peralkaline derivatives. The same holds true for partial melting. The exact position of the redox divide line and its possible dependence on bulk composition require additional experiments. Our data obtained at high fO_2, although relevant to understanding the role of clinopyroxene in silicic magmas, have probably little direct applicability to natural systems, as such extreme fO_2, close to HM, are probably rarely, if ever, reached in magmas. Values of $fO_2 <$ FMQ at temperatures below 800°C favour the development of peralkalinity, in that clinopyroxene crystallization is prevented. Any petrogenetic model invoking melting continental crust to produce peralkaline silicic magmas, as previously argued on geochemical grounds for the Olkaria complex (Davies & Macdonald, 1987; Macdonald *et al.*, 1987; Black *et al.*, 1997; Heumann & Davies, 2002) also requires the establishment of such conditions. However, a peralkaline derivative will form only if the melt is slightly more peralkaline than its coexisting feldspar (Bailey & Schairer, 1964; Bailey & Macdonald, 1969), as our data have illustrated. To produce such a slightly peralkaline melt, a clinopyroxene-bearing, quartzo-feldspathic source, in which clinopyroxene breaks down during melting at low temperature and fO_2, and perhaps high fF_2, can be envisaged. On this basis, fluxing of a reduced quartzo-feldspathic source by fluids having high F contents can conceivably produce anatectic peralkaline melts. This scenario is similar to that proposed by Bailey & Macdonald (1987), except that the excess Na need not be introduced by the incoming fluids.

The plagioclase effect is often considered to be the prime factor leading to the metaluminous–peralkaline transition in magmatic rock suites (Bailey & Schairer, 1966; Barberi *et al.*, 1975). Whereas this mechanism possibly operates in Ca-rich silicic magmas (e.g. Barberi *et al.*, 1975), it may not in Ca-poor types. From a compilation of phase equilibrium data for peraluminous, metaluminous and peralkaline silicic magmas, Scaillet & Macdonald (2001) concluded that plagioclase is intrinsically unstable in Ca-poor peralkaline silicic melts. The clinopyroxene effect is an alternative to the plagioclase effect and it would be worth testing if clinopyroxene has played a similar role in other natural peralkaline series.

Implications for the development of the geochemical trends in Naivasha rhyolites

Our data show that BL575 and SMN49 compositions can be produced by fractionation of magma compositions similar to ND002. On the basis of major element modelling, Macdonald *et al.* (1987) showed that this could be achieved by 82·5 wt % crystallization of an alkali feldspar–quartz–clinopyroxene–titanomagnetite assemblage. Our data indicate that BL575- and SMN49-like melts require ~95–99 wt % crystallization of an ND002-like composition. This is because the

first model assumed, wrongly, that clinopyroxene is part of the fractionating assemblage. At 700°C, 150 MPa, the extreme crystallization or near-solidus melting of ND002 produces a liquid that has an Na/K ratio of 1·28 and a melt water content of 2·4 wt % and coexists with quartz, alkali feldspar, fayalite, ilmenite and biotite (charge 33, Table 1). To produce a comendite having the pre-eruption characteristics of either SMN49 or BL575 (660°C, melt H_2O 5–6 wt %; Scaillet & Macdonald, 2001) requires that such a liquid fractionates so that both the melt peralkalinity and water content increase to the observed values. Another possibility is melting or crystallization near the solidus of ND002 at temperatures lower than 700°C and under conditions richer in water. On the other hand, fractionation of BL575 or SMN49 comendites gives rise to Eburru-type pantellerites (Fig. 2). The latter need not be derived from trachytic parents. We conclude that, at Olkaria at least, strongly peralkaline melts totally comparable in composition with natural pantellerites have formed by crystallization of high-silica comendites of inferred anatectic origin.

ACKNOWLEDGEMENTS

The work has benefited from continuous discussions with Michel Pichavant. We thank Mike Carroll, David Green and an anonymous journal referee for very helpful reviews of an earlier version of the manuscript, as well as Marjorie Wilson for the careful editorial handling.

REFERENCES

Albarède, F. (1995). *Introduction to Geochemical Modeling*. Cambridge: Cambridge University Press, 543 pp.

Ayalew, D., Barbey, P., Marty, B., Reisberg, L., Yirgu, G. & Pik, R. (2002). Source, genesis, and timing of giant ignimbrite deposits associated with Ethiopian continental flood basalts. *Geochimica et Cosmochimica Acta* **66**, 1429–1448.

Bailey, D. K. & Macdonald, R. (1969). Alkali feldspar fractionation trends and the derivations of peralkaline liquids. *American Journal of Science* **267**, 242–248.

Bailey, D. K. & Macdonald, R. (1975). Fluorine and chlorine in peralkaline liquids and the need for magma generation in an open system. *Mineralogical Magazine* **40**, 405–414.

Bailey, D. K. & Macdonald, R. (1987). Dry peralkaline felsic liquids and carbon dioxide flux through the Kenya rift zone. In: Mysen, B. O. (ed.) *Magmatic Processes: Physiochemical Principles*. *Geochemical Society*, *Special Publication* **1**, 91–105.

Bailey, D. K. & Schairer, J. F. (1964). Feldspar–liquid equilibria in peralkaline liquids—the orthoclase effect. *American Journal of Science* **262**, 1198–1206.

Bailey, D. K. & Schairer, J. F. (1966). The system Na_2O–Al_2O_3–Fe_2O_3–SiO_2 at 1 atmosphere, and the petrogenesis of alkaline rocks. *Journal of Petrology* **7**, 114–170.

Barberi, F., Santacroce, R., Ferrara, G., Treuil, M. & Varet, J. (1975). A transitional basalt–pantellerite sequence of fractional crystallisation, the Boina centre (Afar Rift, Ethiopia). *Journal of Petrology* **16**, 22–56.

Black, S., Macdonald, R. & Kelly, M. R. (1997). Crustal origin for peralkaline rhyolites from Kenya: evidence from U-series disequilibria and Th-isotopes. *Journal of Petrology* **38**, 277–297.

Bohlen, S. R. & Essene, E. J. (1978). The significance of metamorphic fluorite in the Adirondacks. *Geochimica et Cosmochimica Acta* **42**, 1669–1678.

Bohrson, W. A. & Reid, M. A. (1997). Genesis of silicic peralkaline volcanic rocks in an ocean island setting by crustal melting and open-system processes: Socorro Island, Mexico. *Journal of Petrology* **38**, 1137–1166.

Bohrson, W. A. & Reid, M. A. (1998). Genesis of evolved ocean island magmas by deep- and shallow-level basement recycling, Socorro Island, Mexico: constraints from Th and other isotopic signatures. *Journal of Petrology* **39**, 995–1008.

Carmichael, I. S. E. (1962). Pantelleritic liquids and their phenocrysts. *Mineralogical Magazine* **33**, 86–113.

Carmichael, I. S. E. & Mackenzie, W. S. (1963). Feldspar–liquid equilibria in pantellerites: an experimental study. *American Journal of Science* **261**, 382–396.

Civetta, L., D'Antonio, M., Orsi, G. & Tilton, G. R. (1998). The geochemistry of volcanic rocks from Pantelleria, Sicily Channel: petrogenesis and characteristics of the mantle source region. *Journal of Petrology* **39**, 1453–1491.

Clarke, M. G. C., Woodhall, D. G., Allen, D. & Darling, G. (1990) Geological, volcanological and hydrogeological controls on the occurrence of geothermal activity in the area surrounding Lake Naivasha, Kenya. Report. Nairobi: Ministry of Energy, 138 pp.

Czamanske, G. K. & Dillett, B. (1988). Alkali amphibole, tetrasilicic mica, and sodic pyroxene in peralkaline siliceous rocks, Questa caldera, New Mexico. *American Journal of Science* **288-A**, 358–392.

Dall'Agnol, R., Scaillet, B. & Pichavant, M. (1999). An experimental study of a lower Proterozoic A-type granite from the Eastern Amazonian craton, Brazil. *Journal of Petrology* **40**, 1673–1698.

Davies, G. R. & Macdonald, R. (1987). Crustal influences in the petrogenesis of the Naivasha basalt–comendite complex: combined trace element and Sr–Nd–Pb constraints. *Journal of Petrology* **28**, 1009–1031.

Devine, J. D., Gardner, J. E., Brack, H. P., Layne, G. D. & Rutherford, M. J. (1995). Comparison of microanalytical methods for estimating water contents of silicic volcanic glasses. *American Mineralogist* **80**, 319–328.

Enders, M., Speer, D., Maresch, W. V. & McCammon, C. A. (2000). Ferric/ferrous iron ratios in sodic amphiboles: Mössbauer analysis, stoichiometry-based model calculations and the high-resolution microanalytical flank method. *Contributions to Mineralogy and Petrology* **140**, 135–147.

Goldsmith, J. R. & Jenkins, D. M. (1985). The high–low albite relations revealed by reversal of degree of order at high pressures. *American Mineralogist* **70**, 911–923.

Goldsmith, J. R. & Newton, B. C. (1974). An experimental determination of the alkali feldspar solvus. In: Mackenzie, W. S. & Zussman, J. (eds) *The Feldspars*. Manchester: Manchester University Press, pp. 337–359.

Hawthorne, F. C. (1976). The crystal chemistry of the amphiboles: V. The structure and chemistry of arfvedsonite. *Canadian Mineralogist* **14**, 346–356.

Henry, C. D., Price, J. G., Rubin, J. N. & Laubach, S. E. (1990). Case study of an extensive silicic lava: the Bracks Rhyolite, Trans-Pecos Texas. *Journal of Volcanology and Geothermal Research* **43**, 113–132.

Heumann, A. & Davies, G. R. (2002). U–Th disequilibrium and Rb–Sr age constraints on the magmatic evolution of peralkaline rhyolites from Kenya. *Journal of Petrology* **43**, 557–577.

Horn, S. & Schmincke, H.-U. (2000). Volatile emission during the eruption of Baitoushan Volcano (China/North Korea) ca. 969 AD. *Bulletin of Volcanology* **61**, 537–555.

Kar, A., Weaver, B., Davidson, J. & Colucci, M. (1998). Origin of differentiated volcanic and plutonic rocks from Ascension Island, South Atlantic Ocean. *Journal of Petrology* **39**, 1009–1024.

Lacroix, A. (1930). Les roches hyperalcalines du massif du Fantalé et du col de Balla. *Mémoires de la Société Géologique de France* **14**, 89–102.

Leake, B. E., *et al*. (1997). Nomenclature of amphiboles. Report of the subcommittee on amphiboles of the International Commission on new minerals and mineral names. *European Journal of Mineralogy* **9**, 623–651.

Lowenstern, J. B. & Mahood, G. A. (1991). New data on magmatic H_2O contents of pantellerites, with implications for petrogenesis and eruptive dynamics at Pantelleria. *Bulletin of Volcanology* **54**, 78–83.

Luth, W. C., Martin, R. F. & Fenn, P. M. (1974). Peralkaline feldpar solvi. In: Mackenzie, W. S. & Zussman, J. (eds) *The Feldspars*. Manchester: Manchester University Press, pp. 297–312.

Macdonald, R. (1974). Nomenclature and petrochemistry of the peralkaline oversaturated extrusive rocks. *Bulletin Volcanologique* **38**, 498–516.

Macdonald, R. (1987). Quaternary peralkaline silicic rocks and caldera volcanoes of Kenya. In: Fitton, J. G. & Upton, B. G. J. (eds) *Alkaline Igneous Rocks. Geological Society, London, Special Publications* **30**, 313–333.

Macdonald, R. & Bailey, D. K. (1973). The chemistry of the peralkaline oversaturated obsidians. *US Geological Survey, Professional Papers* **440-N**(Part 1), 1–37.

Macdonald, R., Bailey, D. K. & Sutherland, D. S. (1970). Oversaturated peralkaline glassy trachytes from Kenya. *Journal of Petrology* **11**, 507–517.

Macdonald, R., Davies, G. R., Bliss, C. M., Leat, P. T., Bailey, D. K. & Smith, R. L. (1987). Geochemistry of high-silica peralkaline rhyolites, Naivasha, Kenya Rift Valley. *Journal of Petrology* **28**, 979–1008.

Macdonald, R., Marshall, A. S., Dawson, J. B., Hinton, R. W. & Hill, P. G. (2002). Chevkinite-group minerals from salic volcanic rocks of the East African Rift. *Mineralogical Magazine* **66**, 287–299.

Mahood, G. A. & Halliday, A. N. (1988). Generation of high-silica rhyolite: a Nd, Sr, and O isotopic study of Sierra La Primavera, Mexican Neovolcanic Belt. *Contributions to Mineralogy and Petrology* **100**, 183–191.

Mahood, G. A. & Stimac, J. A. (1990). Trace-element partitioning in pantellerites and trachytes. *Geochimica et Cosmochimica Acta* **54**, 2257–2276.

Marshall, A. S. (1999). High-silica peralkaline magmatism of the Greater Olkaria Volcanic Complex, Kenya Rift Valley. Ph.D. thesis, Lancaster University.

Martin, R. F. (1974). Controls of ordering and subsolidus phase relations in the alkali feldspar. In: Mackenzie, W. S. & Zussman, J. (eds) *The Feldspars*. Manchester: Manchester University Press, pp. 313–336.

McDonough, W. F. & Nelson, D.O. (1984). Geochemical constraints on magma processes in a peralkaline system: the Paisano volcano, west Texas. *Geochimica et Cosmochimica Acta* **48**, 2443–2455.

Mungall, J. E. & Martin, R. F. (1995). Petrogenesis of basalt–comendite and basalt–pantellerite suites, Terceira, Azores, and some implications for the origin of ocean-island rhyolites. *Contributions to Mineralogy and Petrology* **119**, 43–55.

Mungall, J. E. & Martin, R. F. (1996). Extreme differentiation of peralkaline rhyolite, Terceira, Azores: a modern analogue of Strange Lake, Labrador? *Canadian Mineralogist* **34**, 769–777.

Noble, D. C., Korringa, M. K. & Haffty, J. (1971). Distribution of calcium between alkali feldspar and glass in some highly differentiated silicic volcanic rocks. *American Mineralogist* **56**, 2088–2097.

Novak, S. W. & Mahood, G. A. (1986). Rise and fall of a basalt–trachyte–rhyolite magma system at the Kane Springs Wash Caldera, Nevada. *Contributions to Mineralogy and Petrology* **94**, 352–373.

Parsons, I. (1978). Alkali feldspars: which solvus? *Physics and Chemistry of Minerals* **2**, 199–213.

Robert, J. L. & Maury, R. (1979). Natural occurrence of a (Fe,Mn,Mg) tetrasilicic potassium mica. *Contributions to Mineralogy and Petrology* **68**, 117–123.

Scaillet, B. & Evans, B. W. (1999). The June 15, 1991 eruption of Mount Pinatubo. I. Phase equilibria and pre-eruption P–T–fO_2–fH_2O conditions of the dacite magma. *Journal of Petrology* **40**, 381–411.

Scaillet, B. & Macdonald, R. (2001). Phase relations of peralkaline silicic magmas and petrogenetic implications. *Journal of Petrology* **42**, 825–845.

Scaillet, B., Pichavant, M. & Roux, J. (1995). Experimental crystallisation of leucogranite magmas. *Journal of Petrology* **36**, 663–705.

Smith, I. E. M., Chappell, B. W., Ward, G. K. & Freeman, R. S. (1977). Peralkaline rhyolites associated with andesitic arcs of the southwest Pacific. *Earth and Planetary Science Letters* **37**, 230–236.

Thompson, R. N. & McKenzie, W. S. (1967). Feldspar–liquid equilibria in peralkaline liquids: an experimental study. *American Journal of Science* **265**, 714–734.

Xirouchakis, D. & Lindsley, D. H. (1998). Equilibria among titanite, hedenbergite, fayalite, quartz, ilmenite and magnetite: experiments and internally consistent thermodynamic data for titanite. *American Mineralogist* **83**, 712–725.